https://doi.org/10.5194/egusphere-2024-3614
Preprint. Discussion started: 11 December 2024

Impact of clouds on vegetation albedo quantified by coupling an atmosphere and a vegetation radiative transfer model

Kevin Wolf[1], Evelyn Jäkel[1], André Ehrlich[1], Michael Schäfer[1], Hannes Feilhauer[2,3,4], Andreas Huth[5,6,2], Alexandra Weigelt[7], and Manfred Wendisch[1]

[1]Institute for Meteorology (LIM), Leipzig University, Leipzig, Germany
[2]iDiv German Centre for Integrative Biodiversity Research Halle-Jena-Leipzig, Leipzig, Germany.
[3]Institute for Earth System Science & Remote Sensing, Leipzig University, Leipzig, Germany.
[4]Remote Sensing Centre for Earth System Research, Leipzig University, Leipzig, Germany.
[5]Department of Ecological Modeling, Helmholtz Centre for Environmental Research–UFZ Leipzig, Leipzig, Germany.
[6]Institute for Environmental Systems Research, University of Osnabrück, Osnabrück, Germany.
[7]Systematic Botany and Functional Biodiversity, Institute of Biology, Leipzig University, Germany.

Correspondence: Kevin Wolf (kevin.wolf@uni-leipzig.de)

Abstract. This paper investigates the influence of clouds on vegetation albedo. For this purpose, we use coupled atmosphere-vegetation radiative transfer (RT) simulations combining the library for Radiative transfer (libRadtran) and the vegetation Soil Canopy Observation of Photosynthesis and Energy fluxes (SCOPE2.0) model. Both models are iteratively linked to more realistically simulate cloud–vegetation-radiation interactions above three types of canopies represented by the spherical, erectophile, and planophile leaf angle distributions. The coupled models are applied to simulate solar, spectral and broadband irradiances under cloud-free and cloudy conditions, with the focus on the visible to near-infrared wavelength range from 0.4 to 2.4 µm wavelengths. The simulated irradiances are used to investigate the spectral and broadband effect of clouds on the vegetation albedo. It is found that changes in solar zenith angle and cloud optical thickness are equally important for variations in the vegetation albedo. For solar zenith angles less than 50°–60° the vegetation albedo is increased by clouds by up to 0.1. The greatest albedo increase is observed during the transition from cloud-free to cloud conditions with a cloud optical thickness (τ) of about 6. For larger values of τ the vegetation albedo saturates and increases only slightly. The increase of the vegetation albedo is a result of three effects: (i) dependence of the canopy reflectivity on the direct and diffuse fraction of downward irradiance, (ii) the shift in the weighting of downward irradiance due to scattering and absorption by clouds, and (iii) multiple scattering between the top of canopy and the cloud base. The observed change in vegetation albedo due to cloudiness is parameterized by a polynomial function, representing a potential method to include cloud–vegetation-radiation interactions in numerical weather prediction and global climate models.

1 Introduction

The Earth's surface represents an important boundary between the lithosphere and atmosphere, across which energy fluxes (latent and sensible heat, turbulence, gases, aerosol particles, and radiation) are exchanged. In the context of radiative processes, the spectral surface albedo $\alpha(\lambda)$, with λ the wavelength, determines the extent to which solar radiation is absorbed and reflected

https://doi.org/10.5194/egusphere-2024-3614
Preprint. Discussion started: 11 December 2024

by the Earth's surface. Consequently, α is a central factor that controls the local solar radiative budget. In the visible–near-infrared wavelength range (VNIR, 0.3–1.0 µm), bare, dry soils typically have a high albedo, while vegetated surfaces exhibit a usually lower albedo close to zero, particularly for wavelength shorter than 700 nm. This is a result of the large fraction of absorbed photosynthetically active radiation (PAR, e.g., Qin et al., 2018) within 0.4 to 0.7 µm wavelength (Roderick et al., 2001; Nemani et al., 2003; Dye, 2004; Min, 2005). Conversely, vegetation has a relatively high reflectivity in the shortwave–infrared (SWIR, 1.0–2.5 µm), compared to moist and nutrient rich bare soil (Bowker, 1985). In many cases, natural surfaces are a combination of vegetation on bare soil for which the albedo at the top of canopy (TOC) is often considered as the most relevant surface for atmosphere ground interaction.

The TOC albedo is primarily determined by the vegetated surface components (i.e., leaves, stems, soil, and water content), and the overall canopy structure (Jones and Vaughan, 2010). In addition to the surface and vegetation characteristics, the TOC albedo is influenced by the atmosphere, the presences of clouds which scatter and absorb radiation, and the solar zenith angle. Optically thin clouds allow the incident radiation to pass through and being scattered in the forward direction. The remaining fraction is scattered backwards in the VNIR part of the solar spectrum and absorbed by water vapor in the SWIR. As a consequence, the presence of clouds reduces the amount of radiation in the SWIR part of the spectrum stronger compared to the VNIR part (Warren, 1982). This shifts the relative weighting of the incoming radiation towards shorter wavelengths. Furthermore, scattering at cloud particles leads to an increase in below-cloud diffuse radiation. This is particularly relevant for cloud-vegetation-radiation interactions, given that diffuse radiation is reflected in no particular direction (isotropic), whereas direct radiation is partly diffused and partly reflected in a preferred direction (specular or Fresnel reflection).

The impact of clouds on cloud–surface-radiation interactions with regard to snow and ice surfaces were already investigated in Arctic regions by Wiscombe and Warren (1980), Warren (1982), and Stapf et al. (2020). These authors have demonstrated that an increase in liquid water path (increase in τ) results in an increase in the broadband surface albedo. Although vegetated surfaces have a lower spectral albedo compared to Arctic regions, it can be expected that clouds have a similar effect on the TOC albedo. So far, the impact of clouds on TOC albedo and vegetated areas has been neglected in RT simulations. Previous investigations looked only at the impact of aerosol and molecular scattering, on reflectance measurements over vegetation (Ranson et al., 1985; Deering and Eck, 1987; Liu et al., 1994). Some studies exist, for example by Lyapustin and Privette (1999), Myhre et al. (2005), and Yang et al. (2020) that used atmospheric RT simulations to calculate surface reflectances depending on different ratios of downward direct and diffuse radiation. Still, frequently fixed ratios of direct and diffuse radiation are assumed in reflectance simulations above vegetation (Atzberger, 2004; Kötz et al., 2004; Schaepman-Strub et al., 2006). Therefore, reflectance simulations, which neglect cloud effects, are spectrally distorted compared to, for example, measurements that are performed under cloudy conditions (Schaepman-Strub et al., 2006; Damm et al., 2015). The spectral distortion is a consequence of cloud-radiation interactions including scattering, transmission, or absorption. The relative contribution of these processes depends on the cloud microphysics, cloud morphology, the wavelength of the incident radiation, and the canopy structure.

Various sophisticated atmospheric radiative transfer models (RTMs) exist that allow to include clouds in the simulations. This study will make use of the library for Radiative transfer (libRadtran, Emde et al., 2016). While atmospheric RTMs, for example the MODerate resolution atmospheric TRANsmission model (MODTRAN, Berk et al., 2014), have been coupled

https://doi.org/10.5194/egusphere-2024-3614
Preprint. Discussion started: 11 December 2024

with vegetation RTMs, like the Soil Canopy Observation of Photosynthesis and Energy fluxes version 2 (SCOPE2.0, Yang et al., 2020), non of the previous approaches considered clouds in these simulations. Some studies have either investigated the radiative effects of clouds over different land types and changing forests (Betts, 2000; Bounoua et al., 2002; Cerasoli et al., 2021), while other studies have concentrated on the RT within or at TOC, taking into account the properties of the canopy itself (Sinoquet et al., 2001; Majasalmi and Rautiainen, 2020; Henniger et al., 2023). As a result of this discussion, there are two question to be addressed in this paper:

i How strongly do clouds impact the spectral and broadband albedo of vegetation?

ii To what extent do leaf area index and leaf angle distribution control cloud–vegetation-radiation interactions?

To answer the two questions listed above and to systematically investigate cloud–vegetation-radiation interactions, we have coupled iteratively the atmospheric RTM libRadtran and the vegetation RTM SCOPE2.0 to investigate the radiative interaction of clouds and vegetation. This coupling is introduced in Section 2 by first defining the fundamental properties to describe the RT in the atmosphere and vegetation, and its interaction with the surface. Then the general set up of the coupling is outlined and the basics of the RT models libRadtran and SCOPE2.0 are introduced. The coupling itself is realized by an iterative approach that is applied for different test cases. Section 3 presents the simulations, focusing on the spectral albedo and the broadband albedo over forest canopies. The results are summarized in Section 4.

2 Terminology, radiative transfer simulations, and iterative coupling

2.1 Terminology

We provide the basic radiometric definitions, terminology, and abbreviations that mainly follow Wendisch and Yang (2012), Schaepman-Strub et al. (2006), and Jones and Vaughan (2010) to facilitate the understanding of this paper.

Radiant energy passing through an area element within a certain time interval that stems from within a certain solid angle element is defined as the spectral radiance $I(\lambda)$ in units of W $\mathrm{m^{-2}\ nm^{-1}\ sr^{-1}}$. The spectral irradiance $F(\lambda)$ is defined by the radiant energy passing through an area element within a certain time interval. $F(\lambda)$ is given in units of W $\mathrm{m^{-2}\ nm^{-1}}$ and can be split into the upward $F^{\uparrow}(\lambda)$ and downward $F^{\downarrow}(\lambda)$ component. Both are defined with respect to a horizontal surface area from either the lower or upper hemisphere, respectively. $F^{\downarrow}(\lambda)$ is composed of the direct solar irradiance $F^{\downarrow}_{\mathrm{dir}}(\lambda)$, transmitted through the atmosphere without any interaction, and the diffuse irradiance $F^{\downarrow}_{\mathrm{dif}}(\lambda)$, which was at least once scattered by atmospheric constituents, and thus:

$$F^{\downarrow}(\lambda) = F^{\downarrow}_{\mathrm{dir}}(\lambda) + F^{\downarrow}_{\mathrm{dif}}(\lambda). \qquad (1)$$

The direct fraction $F^{\downarrow}_{\mathrm{dir}}(\lambda)$ in relation to $F^{\downarrow}(\lambda)$ is quantified by the ratio $f_{\mathrm{dir}}(\lambda)$ defined by:

$$f_{\mathrm{dir}}(\lambda) = F^{\downarrow}_{\mathrm{dir}}(\lambda)/F^{\downarrow}(\lambda) = 1 - F^{\downarrow}_{\mathrm{dif}}(\lambda)/F^{\downarrow}(\lambda). \qquad (2)$$

https://doi.org/10.5194/egusphere-2024-3614
Preprint. Discussion started: 11 December 2024

In theory, the ratio $f_{\mathrm{dir}}(\lambda)$ ranges between a value of 0, indicating no direct radiation, and a value of 1, indicating pure direct radiation. However, pure direct radiation is unrealistic under normal atmospheric conditions.

Calculating the ratio between $F^{\uparrow}(\lambda)$ and $F^{\downarrow}(\lambda)$ yields the spectral albedo $\alpha(\lambda)$ (unitless) given by:

$$\alpha(\lambda) = \frac{F^{\uparrow}(\lambda)}{F^{\downarrow}(\lambda)}. \tag{3}$$

The broadband albedo α_{BB} (unitless) is obtained by weighting the spectral albedo with $F^{\downarrow}(\lambda)$ by:

$$\alpha_{\mathrm{BB}} = \frac{\int_{0.2\,\mu\mathrm{m}}^{4.5\,\mu\mathrm{m}} \alpha(\lambda) \cdot F^{\downarrow}(\lambda)\,\mathrm{d}\lambda}{\int_{0.2\,\mu\mathrm{m}}^{4.5\,\mu\mathrm{m}} F^{\downarrow}(\lambda)\,\mathrm{d}\lambda} \tag{4}$$

and integrating over the wavelength range from 0.2 to 4.5 µm. Broadband α_{BB} is equivalent to measurements with broadband albedometers, i.e., a set of upward and downward looking pyranometers. In the following the integration of $\alpha(\lambda)$ is limited to the wavelength range from 0.4 to 2.4 µm. Often, natural surfaces, such as forests, are a combination of vegetation on bare ground for which the albedo at the TOC is often considered to be the most relevant surface for atmosphere–ground-interaction. In this case, the albedo at the TOC is simply referred to as the albedo $\alpha(\lambda)$. In the special case that we refer to the albedo of the bare ground, we indicate this by the subscript "srf", denoted by $\alpha_{\mathrm{srf}}(\lambda)$.

The primary parameter that describes the radiative properties of a canopy is the leaf area index (LAI, Watson, 1947; Asner, 1998; Jones and Vaughan, 2010). It is a measure for the total one-sided area of leaves per unit ground area given in units of $\mathrm{m}^2\,\mathrm{m}^{-2}$, and can range between values from 0 to 12. The LAI depends on vegetation type and is subject to annual and seasonal variations as well as weather and climate conditions (Eugster et al., 2000; Davidson and Wang, 2004, 2005).

The second most important parameter that controls the RT in the canopy is the leaf angle distribution (LAD, Baldocchi et al., 2002; Jones and Vaughan, 2010; Verrelst et al., 2015; Yang et al., 2023). The LAD ultimately determines the sunlit area of a leaf with respect to the one-sided total leaf area and, thus, the area where reflection and absorption occurs (Asner, 1998; Stuckens et al., 2009; Vicari et al., 2019). The leaf angle of an individual leaf is defined as the angle between the leaf normal and the zenith. Goel (1988) proposed six LADs, with three common types: the spherical distribution, where all leave orientations have the same probability; the erectophile distribution, where the majority of leaves have a preferred vertical alignment; and the planophile distribution, where most of the leaves are horizontally aligned. The erectophile and planophile LAD represent two extreme cases among the LADs. Within models, LADs are described by two-parameter beta distributions, trigonometric functions, or ellipsoidal distributions (Goel and Strebel, 1984; Jones and Vaughan, 2010).

The extinction of radiation by scattering and absorption in homogeneous media can be approximated by the turbid medium model (Kubelka, 1931; Kokhanovsky, 2009; Jones and Vaughan, 2010). Within the Earth's atmosphere, scattering and absorption by clouds, aerosol particles, and gas molecules is quantified by the cloud optical thickness $\tau(\lambda)$, which depends on the volumetric extinction coefficient $\beta_{\mathrm{ext}}(\lambda)$ (given in units of m^{-1}). In the simplified case of a homogeneous atmosphere, the extinction of direct solar radiation follows the Lambert–Beer–Bougier-law, which can be expressed as:

$$\tau(\lambda, z) = \beta_{\mathrm{ext}}(\lambda) \cdot z, \tag{5}$$

https://doi.org/10.5194/egusphere-2024-3614
Preprint. Discussion started: 11 December 2024

with the path length z. The extinction of $I(\lambda)$ at z is then expressed by:

$$\frac{I(\lambda)_z}{I(\lambda)_0} = e^{-b_{\mathrm{ext}}(\lambda)\cdot z} = e^{-\tau(\lambda)}, \quad (6)$$

where $I(\lambda)_0$ is the direct radiance at the top of atmosphere (TOA), $I(\lambda)_z$ is the direct radiance at a certain penetration depth with $z = 0$ at TOA. Monsi (1953) proposed a similar concept to treat the RT in homogeneous vegetation. Attenuation of direct radiance at penetration depth z is then caused by leaves, which are considered as point scatterers (Kubelka, 1931; Jones and Vaughan, 2010). In literature concerning vegetation RT, the extinction coefficient $\beta_{\mathrm{ext}}(\lambda)$ in Eq. 5 and Eq. 6 is replaced by k_{ext} here called the vegetation extinction coefficient. The penetration depth z is also replaced with the LAI. A brief overview about estimated of k_{ext} and approximated $I(\lambda)$ within vegetation can be found in Section C in the Appendix.

2.2 Iterative coupling

The reflectance and albedo of a surface are primarily controlled by the structural parameters of the vegetation but are also driven by atmospheric factors, namely the direct and diffuse components of the incident radiation $F^{\downarrow}(\lambda)$, and the angle of the incident radiation on the surface. It is noted that the incident angle, in the following referred to as θ, is not necessarily equal to the solar zenith angle θ_0. Both angles are approximately equal for cloud-free atmospheres and low aerosol particle concentrations but increasingly deviate for overcast conditions (e.g., see Wiscombe and Warren (1980)). Even though the effects of canopy structure (vegetation) and clouds (atmosphere) on the RT are known, vegetation and atmosphere RT models are run separately. Atmospheric RMTs often rely on standard libraries of forest albedo, such as the library of the International Geosphere Biosphere Programme (IGBP; Loveland and Belward, 1997). Conversely, vegetation RTMs do simulate the RT in and directly above the canopy but neglect scattering and absorption by clouds in the atmosphere, and assume a fixed ratio of direct to diffuse ratio of $F^{\downarrow}(\lambda)$. By iteratively coupling vegetation and atmospheric RTMs, the atmospheric RTM provides more realistic solar spectra of $F^{\downarrow}_{\mathrm{dir}}(\lambda)$ and $F^{\downarrow}_{\mathrm{dif}}(\lambda)$, while the vegetation RTM provides a more realistic albedo above canopies that is used as input for the atmosphere RTM. In the proposed setup, the iterative coupling of the vegetation and atmosphere RTMs is achieved through the exchange of $F^{\downarrow}_{\mathrm{dir}}(\lambda)$ and $F^{\downarrow}_{\mathrm{dif}}(\lambda)$, and $\alpha(\lambda)$ between the two models. More specifically, $F^{\downarrow}_{\mathrm{dir}}(\lambda)$ and $F^{\downarrow}_{\mathrm{dif}}(\lambda)$ simulated by the atmosphere RTM provide the input to the vegetation RTM. Then the simulated $F^{\uparrow}(\lambda)$, in combination with $F^{\downarrow}_{\mathrm{dir}}(\lambda)$ and $F^{\downarrow}_{\mathrm{dif}}(\lambda)$ from the atmosphere RTM, allows an updated $\alpha(\lambda)$ to be calculated and used as input for the next simulation with the atmosphere RTM.

Figure 1 shows a schematic of the proposed iterative coupling. Each simulation run is realized by n iterations, where each iteration includes a calculation from the atmospheric RT (blue box) and the vegetation RT (green box). The first iteration starts with the atmospheric RTM, using a first guess, spectral surface albedo of forests, here the "mixed forest" spectral surface albedo from the IGBP database. The simulated upward and downward $F_n(\lambda)$ of the first simulation (n = 0). The direct and diffuse components of $F^{\downarrow}_n(\lambda)$ are then ingested in the vegetation RTM, which is therefore initialized with $F^{\downarrow}_n(\lambda)$ representing the atmospheric conditions including clouds, instead of a default $F^{\downarrow}(\lambda)$ and direct–diffuse-ratio. The new $F^{\uparrow}_{n+1}(\lambda)$ from the vegetation RTM is then used to calculate $\alpha_{n+1}(\lambda)$ at TOC using Eq. 3. The updated surface albedo provides the input for the atmospheric RTM in the next iteration step. We call an iteration successfully converged if the relative difference between

https://doi.org/10.5194/egusphere-2024-3614
Preprint. Discussion started: 11 December 2024

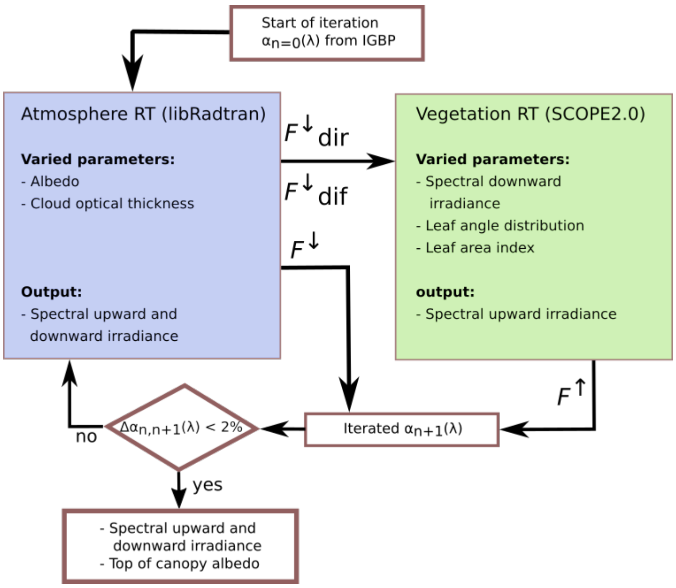

Figure 1. Schematic of coupled atmosphere (blue) and vegetation (green) radiative transfer model (RTM). The RMTs are coupled via the exchange of spectral, direct $F^{\downarrow}_{\mathrm{dir}}(\lambda)$ and diffuse $F^{\downarrow}_{\mathrm{dif}}(\lambda)$ downward irradiance, and the top-of-canopy albedo $\alpha(\lambda)$. The atmospheric RTM is started with a first guess albedo from the IGBP database. When the convergence criteria is met, the iteration is stopped.

iteration n and $n+1$ for 90 % of the wavelengths is less than 2 % for the albedo. Formalized, this can be expressed as:

$$P_{90^{th}}\left(\frac{|\alpha_n(\lambda)-\alpha_{n+1}(\lambda)|}{\alpha_{n+1}(\lambda)}\right) < 0.02 \quad (7)$$

with $P_{90^{th}}$ the 90^{th} percentile, the spectral albedo $\alpha_n(\lambda)$ of the previous iteration step, and the spectral albedo $\alpha_{n+1}(\lambda)$ of the current iteration. In this study two iterations were found to be sufficient for all canopy and cloud parameter combinations. This is consistent with Wendisch et al. (2004), who also used an iterative approach to determine the surface albedo from airborne observations. They found that after two iterations, even for rough estimates of $\alpha(\lambda)$, the retrieved albedo is close to the true surface albedo. Furthermore, in most applications the surface albedo is approximately known, e.g., from the IGBP data base, which provides an even better initial guess and reduces the number of required iterations.

2.2.1 Atmospheric radiative transfer model libRadtran

The atmospheric RTM library for Radiative transfer (libRadtran, Emde et al., 2016) has been applied to simulate the RT through the atmosphere above the canopy. The 1-dimensional solver "Discrete-Ordinate-Method Radiative Transfer" (DISORT, Stamnes et al., 1988; Buras et al., 2011) was selected to calculated the RT using 12 streams, which is supposed to be sufficient to study irradiances. Clouds were assumed to be homogeneous. Spectral calculations of $F^{\uparrow}(\lambda)$ and $F^{\downarrow}(\lambda)$ were performed for a wavelength range from 0.4 to 2.4 µm, which were also used as the limits for integrated $F_{\mathrm{BB,sol}}$. The incoming spectral irradiance at TOA was represented by the solar reference spectrum provided by Coddington et al. (2021). Molecular absorption

https://doi.org/10.5194/egusphere-2024-3614
Preprint. Discussion started: 11 December 2024

was considered by using the "medium" resolution parameterization from Gasteiger et al. (2014). A default aerosol distribution after Shettle (1989) was applied, which represents aerosol of rural type in the boundary layer, back-ground aerosol above 2 km during spring-summer, and a visibility of 50 km. Atmospheric profiles of air temperature, humidity, and gas concentrations were represented by the mid-latitude summer profile 'afglms' after Anderson et al. (1986). Absorption by water vapor and other atmospheric trace gases were included in the simulations (Anderson et al., 1986; Emde et al., 2016). Low- and mid-level warm stratus and altostratus were represented by liquid water clouds with a fixed cloud base at 3 km altitude and a cloud top altitude of 3.5 km. The cloud droplet effective radius was fixed to 10 µm (Stephens, 1994; Frisch et al., 2002; Aebi et al., 2020). The liquid water path was modified such that a desired value of $\tau(\lambda = 550\,\mathrm{nm})$ at 550 nm is achieved and all other values are scaled accordingly, considering the wavelength dependence of τ. Subsequently, $\tau(\lambda = 550\,\mathrm{nm})$ is referred to as τ for simplicity. The initial run of libRadtran was initialized with the "mixed-forest" albedo α taken from the IGBP data base, which was then replaced by $\alpha(\lambda)$ from SCOPE2.0. An output altitude of 40 m above ground was selected to characterize the downward radiation (direct and diffuse) just above the canopy.

2.2.2 Vegetation radiative transfer model SCOPE2.0

The solar RT through vegetation was simulated with the Soil Canopy Observation of Photosynthesis and Energy fluxes (SCOPE2.0 Yang et al., 2021). SCOPE2.0 is an updated version of SCOPE, which has been developed for forward modeling radiances and albedo for satellite vegetation retrievals. SCOPE2.0 treats the RT by combining the leaf RTM PROperties SPECtra (PROSPECT) with the canopy RTM Scattering by Arbitrarily Inclined Leaves (SAIL Verhoef, 1984; Yang et al., 2017, 2021). At their core, these models base on the turbid medium approach (Yan et al., 2021). In SCOPE2.0 the ground albedo assumes surfaces of different moisture, where the moisture dependence is determined by the Brightness-Shape-Moisture (BSM) model (Verhoef et al., 2018; Yang et al., 2020). The default BSM model parameter for soil brightness B = 2 was used. The optical properties of individual leaves are provided by the Fluorescence spectra (Fluspect) model, which developed out of PROSPECT (Vilfan et al., 2016, 2018). The upward directed $F^{\uparrow}(\lambda)$ and the canopy albedo at TOC was simulated as a superposition of the soil and the contribution from the vegetation. Simulations in the solar part of the spectrum with SCOPE2.0 are generally limited to the wavelength range from 0.4 to 2.4 µm. Consequently, the calculation of spectral $\alpha(\lambda)$ and broadband albedo α_{BB} were restricted to the same wavelength range, where α_{BB} was calculated with Eq. 4. The optical properties of vegetation primarily depend on the vegetation type, tree species, tree age, canopy structure, and the solar zenith angle (Liang et al., 2005; Stenberg et al., 2013; Hovi et al., 2017; Zheng et al., 2019). To consider different vegetation states during the annual cycle, the LAI was varied between 2 and 5 $\mathrm{m^2\,m^{-2}}$, with LAI = 3 $\mathrm{m^2\,m^{-2}}$ as the default. In SCOPE2.0 the LAD is represented by a linear combination of trigonometric functions in the leaf inclination distribution function (LIDF) (Verhoef, 1998), which is specified by the two parameters LIDF_a and LIDF_b. Three different LAD - spherical, planophile, and erectophile - were simulated. The parameters LIDF_a and LIDF_b for the three LADs are provided in Table 1. Table 2 summarizes the relevant parameters for vegetation RT simulations in the visible–near-infrared wavelength range that were kept constant in the simulations.

https://doi.org/10.5194/egusphere-2024-3614
Preprint. Discussion started: 11 December 2024

Table 1. Leaf angle distribution (LAD) and corresponding values for the leaf inclination distribution function parameters LIDF_a and LIDF_b that were used to parameterize the orientation of the leaves (Yang et al., 2021).

Distribution	LIDF_a	LIDF_b	exemplary specie		Reference
spherical	-0.35	-0.15	*Tilia cordata*	Small-leaved linden, broadleaf	Pisek et al. (2022)
planophile	1.0	0.0	*Quercus robur*	English oak, broadleaf	Pisek et al. (2022)
erectophile	-1.0	0.0	*Ostrya japonica*	Japanese hop-hornbeam, broadleaf	Vicari et al. (2019)

Table 2. Selected configuration of the SCOPE2.0 simulations.

Description	Symbol	Setting	Unit
leaf chlorophyll concentration	C_{ab}	40	µg cm^{-2}
leaf carotenoid concentration	C_{ca}	10	µg cm^{-2}
leaf water equivalent layer	C_{w}	0.009	cm
leaf structure parameter	N	1.5	Unitless
BSM model parameter for soil brightness	B	0.5	Unitless
vegetation height	h_{c}	20	m
output height	h_{out}	40	m

3 Results

The coupled simulations were performed for a range of cloud conditions from cloud-free (τ = 0) to overcast (τ = 80). It was found that the sensitivity of the simulated spectral and broadband $F(\lambda)$ and $\alpha(\lambda)$ was greatest below τ = 6, thus, defining the range of this study. Section B in the Appendix provides a brief discussion of the response of α_{BB} for τ > 6.

The benefit of coupled atmosphere and vegetation RTM on $F^{\downarrow}(\lambda)$ and $\alpha(\lambda)$ is demonstrated in Fig. 2a and b, which show an example of $F^{\downarrow}_{\mathrm{dif}}(\lambda)$ and $\alpha(\lambda)$ at different stages of the iteration, respectively. The simulations are performed for an intermediate SZA of 45° and a value of τ = 2. Figure 2a focuses on the diffuse component $F^{\downarrow}_{\mathrm{dif}}(\lambda)$, since $F^{\downarrow}_{\mathrm{dir}}(\lambda)$ is not affected by multiple scattering from the canopy. Under cloud-free conditions (black line), downward diffuse irradiance $F^{\downarrow}_{\mathrm{dif}}(\lambda)$ above the canopy is generally small, with a slight increase below 700 nm toward shorter wavelengths due to the increasing contribution of Rayleigh scattering. Including clouds in the atmospheric RTM increases $F^{\downarrow}_{\mathrm{dif}}(\lambda)$ (red line) compared to the cloud-free case

https://doi.org/10.5194/egusphere-2024-3614
Preprint. Discussion started: 11 December 2024

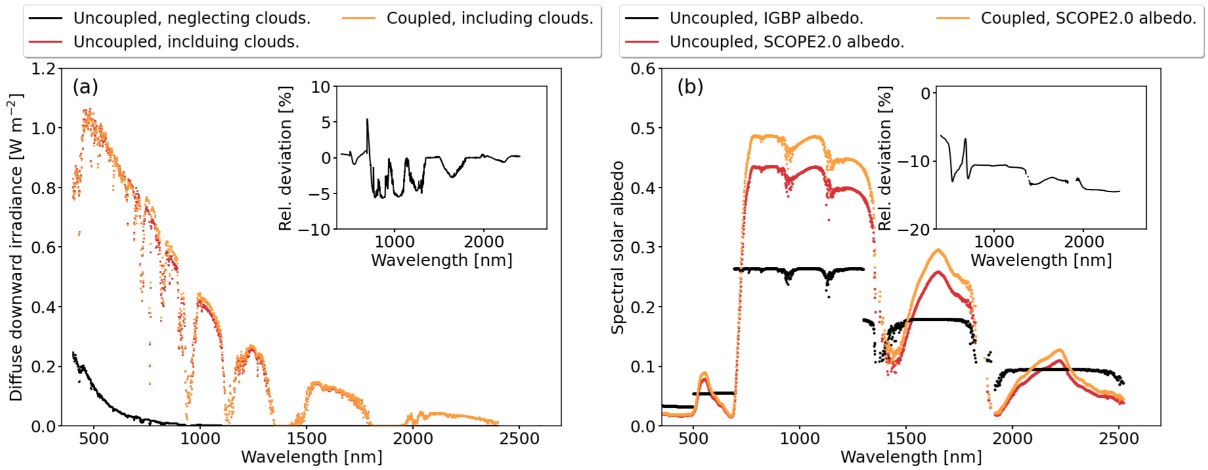

Figure 2. (a) Simulated diffuse, downward spectral irradiance $F^{\downarrow}_{\mathrm{dif}}(\lambda)$. In black: $F^{\downarrow}_{\mathrm{dif}}(\lambda)$ simulated for cloud-free conditions (τ = 0) and for uncoupled models. In red: $F^{\downarrow}_{\mathrm{dif}}(\lambda)$ simulated for a value of τ = 4 but still in the uncoupled set-up. In orange: $F^{\downarrow}_{\mathrm{dif}}(\lambda)$ from coupled simulation for a value of τ = 4. **(b)** Simulated spectral albedo $\alpha(\lambda)$. In black: $\alpha(\lambda)$ simulated using the "mixed-forest" albedo from the IGBP data base and uncoupled simulations. In red: $\alpha(\lambda)$ coupled simulation but neglecting clouds. In orange: $\alpha(\lambda)$ from the coupled simulation including clouds with τ = 4. Subplots show respective relative differences with respect to the coupled simulations (orange lines).

due to scattering at cloud particles. The spectra is characterized by water vapor absorption in the wavelength bands of 933–946 nm, 1118–1144 nm, 1350–1480 nm, and 1810–1959 nm. Coupling libRadtran and SCOPE2.0 iteratively results in $F^{\downarrow}_{\mathrm{dif}}(\lambda)$ (orange line) which is slightly higher compared to the uncoupled simulations. The largest relative differences of up to 5 % between uncoupled and coupled simulations (with respect to the fully coupled simulations) occur between 700 and 1200 nm wavelengths, where the total $F^{\downarrow}$ and $\alpha(\lambda)$ are largest (see Fig. 2a subpanel). Thus, a larger fraction of $F^{\uparrow}(\lambda)$ that is reflected from the TOC contributes to $F^{\downarrow}_{\mathrm{dif}}(\lambda)$.

Since clouds generally change $F^{\downarrow}(\lambda)$, they also affect $\alpha(\lambda)$. Figure 2b shows three simulated $\alpha(\lambda)$ over vegetation during different stages of the coupling. A generic $\alpha(\lambda)$ is provided by the IGBP data base (black line), which was used to initialize the libRadtran simulations. The radiation is reflected isotropically and does not take into account any dependence on the incident angle nor the presence of clouds. A spectrally higher resolved vegetation $\alpha(\lambda)$ was obtained after the first simulation with SCOPE2.0 (red line). Simulations at this stage of the iteration account for the optical properties of the canopy but still neglected clouds and cloud–vegetation-radiation interactions. Coupling both models resulted in $\alpha(\lambda)$ given by the orange line, which is higher compared to the uncoupled simulations. For the example presented, the relative differences between the uncoupled, cloud-free and coupled, cloudy SCOPE2.0 simulations are between 12 and 16 % depending on the wavelength (see subpanel Fig. 2b). The relative differences were calculated with respect to the fully coupled simulations.

The differences in the spectral and broadband $F(\lambda)$ and α between uncoupled and coupled simulations depend on θ_0 and the optical properties of the clouds and the vegetation, which are systematically analyzed in the following.

https://doi.org/10.5194/egusphere-2024-3614
Preprint. Discussion started: 11 December 2024

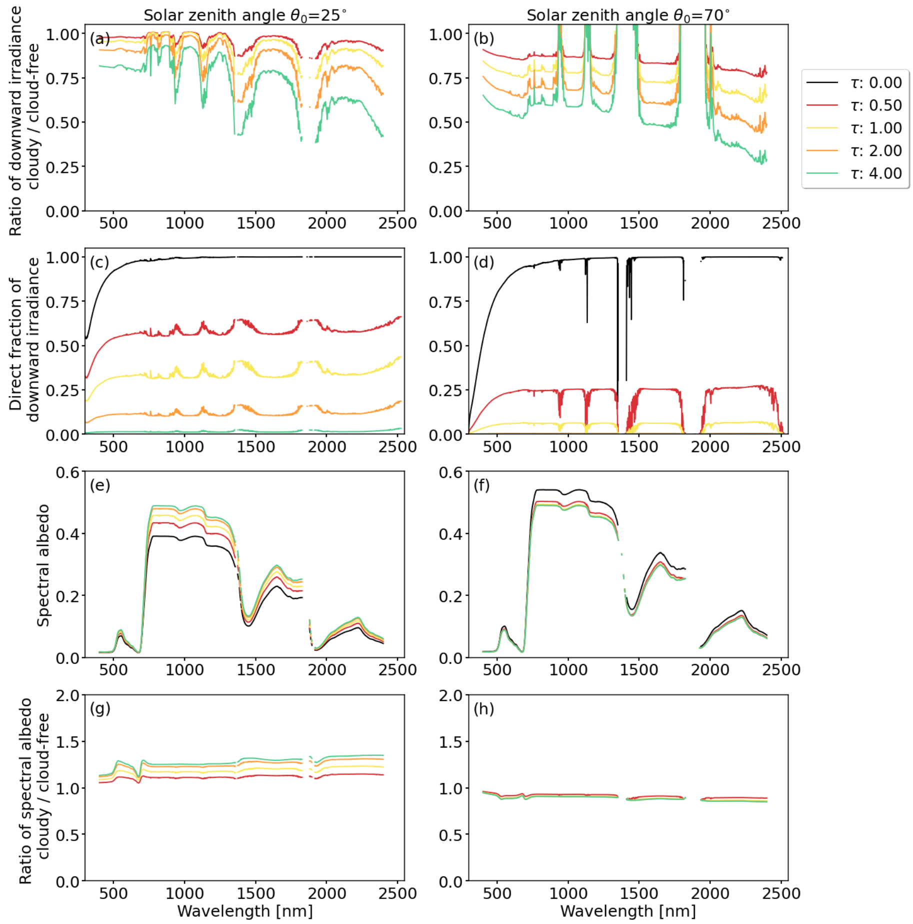

Figure 3. Simulations for a solar zenith angle $\theta_0 = 25°$ (left column) and $\theta_0 = 70°$ (right column), and a leaf area index LAI = 3. Cloud optical thickness τ is indicated by the colored lines. From top to bottom: **(a,b)** Ratio $F^{\downarrow}_{\mathrm{c}}(\lambda)/F^{\downarrow}_{\mathrm{cf}}(\lambda)$ (unitless) of spectral downward irradiance $F^{\downarrow}(\lambda)$ under cloudy conditions (index c) in relation to cloud-free conditions (index cf). **(c,d)** Direct fraction $f_{\mathrm{dir}}(\lambda)$ of total downward irradiance $F^{\downarrow}(\lambda)$. **(e,f)** Spectral albedo $\alpha(\lambda)$ (unitless). **(g,h)** Ratio $\alpha_{\mathrm{c}}(\lambda)/\alpha_{\mathrm{cf}}(\lambda)$ (unitless) of spectral α under cloudy conditions (index c) in relation to cloud-free conditions (index cf).

3.1 Spectral sensitivity of surface albedo on solar zenith angle, cloud optical thickness, and leaf angle distribution

Radiation that interacts with clouds is scattered and absorbed. Wavelengths below 900 nm that are outside the absorption bands are primarily affected by scattering from molecules, aerosol, and cloud particles (Mie, 1908), while absorption dominates the longer wavelengths. An example of simulated direct and diffuse $F^{\downarrow}(\lambda)$ for four different values of τ is given in Section A in the Appendix. Here we express the wavelength-dependent effects of scattering and absorption on the total $F^{\downarrow}(\lambda)$ by the ratio $F^{\downarrow}_{\mathrm{c}}(\lambda)/F^{\downarrow}_{\mathrm{cf}}(\lambda)$, where $F^{\downarrow}_{\mathrm{c}}(\lambda)$ represents cloudy (index "c") simulations, while $F^{\downarrow}_{\mathrm{cf}}(\lambda)$ represents cloud-free (index "cf") simulations. The ratio visualizes the differences between the two conditions. Most importantly, all simulations of $F^{\downarrow}_{\mathrm{cf}}(\lambda)$ where

https://doi.org/10.5194/egusphere-2024-3614
Preprint. Discussion started: 11 December 2024

τ = 0, simultaneously represent simulations that neglect the presence of clouds and, for example, only consider a standard atmospheric profile in the vegetation RT simulations. Thus, the ratio provides a measure of the difference between simulations neglecting and including clouds in the RT simulations.

Figure 3a and b show the ratio $F_{\mathrm{c}}^{\downarrow}(\lambda)/F_{\mathrm{cf}}^{\downarrow}(\lambda)$ for the extreme cases of θ_0 of 25° and 70°, respectively. The presence of clouds results in a ratio $F_{\mathrm{c}}^{\downarrow}(\lambda)/F_{\mathrm{cf}}^{\downarrow}(\lambda)$ that is less than 1, since radiation is scattered at the cloud top and absorbed inside the cloud. For the same cloud, a value of θ_0 =70° results in a smaller ratio compared to θ_0 =25° due to the longer path length through the cloud, which increases extinction. With increasing solar zenith angle θ_0, even small variations in τ do have an increasing effect on $F_{\mathrm{c}}^{\downarrow}(\lambda)/F_{\mathrm{cf}}^{\downarrow}(\lambda)$ due to the cosine dependence on θ_0. The extinction of radiation by absorption at longer wavelengths is greater than by scattering at shorter wavelengths. Relatively speaking, the decrease in the radiation above the cloud compared to the radiation below the cloud is more pronounced at longer wavelengths. This results in a spectral slope in $F_{\mathrm{c}}^{\downarrow}(\lambda)/F_{\mathrm{cf}}^{\downarrow}(\lambda)$ that steepens from shorter to longer wavelengths. The spectral slope becomes more pronounced with increasing τ and θ_0, and is indicative of a shift in the weighting of incoming radiation from longer to shorter wavelengths (Wiscombe and Warren, 1980; Grenfell and Perovich, 2008). To illustrate, an increase in τ from 0 to 1 (yellow line) results in a ratio of 0.95 at 500 nm and a ratio of about 0.9 at 1600 nm. Increasing τ from 0 to 4 (light green line) results in ratios of 0.75 at 500 nm and 0.65 at 1600 nm wavelengths.

Scattering at clouds changes the fraction $f_{\mathrm{dir}}(\lambda)$ of direct radiation, which determines how radiation is reflected by a surface. Non-isotropic, also called non-Lambertian surfaces, reflect diffuse radiation mostly in a diffuse manner. In contrast, direct radiation reflected by non-isotropic surfaces has a preferred direction that depends on the incident angle and the inherent reflective properties of the surface (Wiscombe and Warren, 1980; Warren, 1982; Grant, 1987; Martonchik et al., 2009). Figure 3c and d show $f_{\mathrm{dir}}(\lambda)$ for θ_0 = 25° and θ_0 = 70°, respectively. Independent of τ, $f_{\mathrm{dir}}(\lambda)$ is sensitive to the wavelengths below 700 nm due to Rayleigh scattering, while $f_{\mathrm{dir}}(\lambda)$ remains relatively constant for wavelengths above 700 nm and can be considered as almost wavelength independent. The direct fraction depends on τ, which gets more sensitive with increasing θ_0 due to the longer path lengths of radiation trough the cloud.

Figure 3e and f show $\alpha(\lambda)$ for θ_0 = 25° and θ_0 = 70°, respectively, and a the spherical LAD. Here, $\alpha(\lambda)$ was calculated with the spherical LAD. The change of $\alpha(\lambda)$ is quantified by the ratio of $\alpha_{\mathrm{c}}(\lambda)/\alpha_{\mathrm{cf}}(\lambda)$ between cloudy and cloud-free conditions and given in Fig 3g and h. Please recall, $\alpha_{\mathrm{cf}}(\lambda)$ represent cloud-free conditions but also simulations that simply neglect clouds in the atmospheric RT. The sign and magnitude of the response of $\alpha(\lambda)$ to τ dependents on θ_0. For a small value of θ_0 = 25°, the spectral albedo increases compared to the cloud-free simulations, indicated by a ratio $\alpha_{\mathrm{c}}(\lambda)/\alpha_{\mathrm{cf}}(\lambda)$ that is always greater than one and approximately constant over the entire wavelength range. With increasing τ (decreasing $f_{\mathrm{dir}}(\lambda)$) the extinction of $F_{\mathrm{dir}}^{\downarrow}(\lambda)$ and its angular dependence on θ_0 in the canopy becomes less important as $F_{\mathrm{dif}}^{\downarrow}(\lambda)$ dominates. For the optically thinnest cloud ($\tau = 0.5$) the enhancement is about 10 %. The maximum enhancement for the optically thickest cloud ($\tau = 5$) is between 25 % (864 nm) and up to 40 % (2400 nm) compared to the cloud-free state. For further increasing τ the change in $\alpha(\lambda)$ becomes smaller and reaches an asymptotic value. For θ_0 = 70°, $f_{\mathrm{dir}}(\lambda)$ is low even for small values of τ and the impact on $\alpha(\lambda)$ is only minor in the presented case. For all values of τ, the ratio $\alpha_{\mathrm{c}}(\lambda)/\alpha_{\mathrm{cf}}(\lambda)$ is smaller than one, indicating a decrease

https://doi.org/10.5194/egusphere-2024-3614
Preprint. Discussion started: 11 December 2024

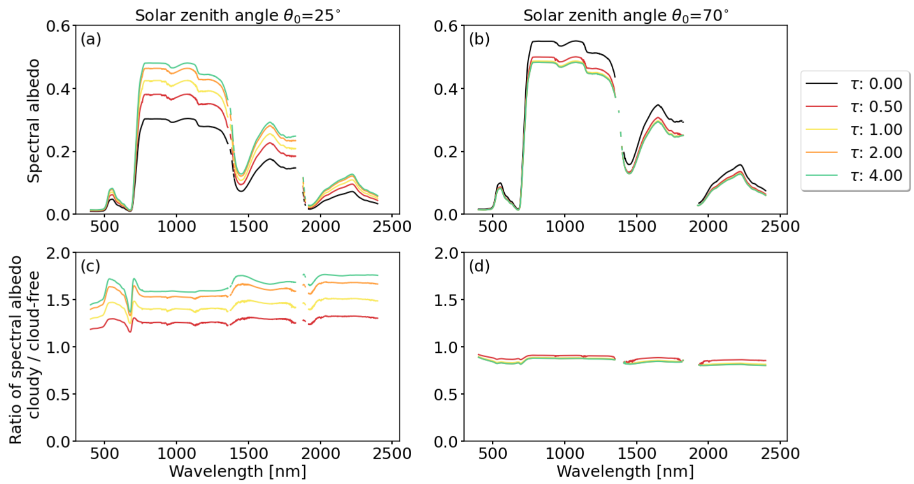

Figure 4. Simulations for solar zenith angles of θ_0 = 25° (left column) and θ_0 = 70° (right column), and a leaf area index LAI = 3. Cloud optical thickness τ is indicated by the colored lines. From top to bottom: **(a,b)** Spectral albedo $\alpha(\lambda)$ (unitless). **(c,d)** Ratio $\alpha_\mathrm{c}(\lambda)/\alpha_\mathrm{cf}(\lambda)$ (unitless) of spectral α under cloudy conditions (index c) in relation to cloud-free conditions (index cf).

of $\alpha(\lambda)$ with increasing τ. The decrease is attributed to the lower directional reflectivity of diffuse radiation compared to direct radiation under same illumination geometry.

Canopies with predominantly vertically oriented leaves are best described by the erectophile LAD. The vertical orientation of the leaves reduces the probability of a photon interacting with the leaves and being scattered out of the canopy at TOC (Ollinger, 2011). The lower probability is expressed in the vegetation extinction coefficient k_ext, which is lower for the erectophile than for the spherical LAD for θ_0 below 52° (see right column in Table C1 and Eq. 6). In cloud-free conditions, the deeper penetration depth also increases the probability of the radiation being absorbed by the surface. Consequently, $\alpha(\lambda)$ for θ_0 = 25° (Fig. 4a) was generally lower compared to the spherical LAD (Fig. 3e) particularly for the cloud-free case, also leads to a greater variability in $\alpha(\lambda)$ under θ_0 = 25° compared to the spherical LAD. In cloud-free conditions, $\alpha(\lambda)$ at 850 nm is approximately 0.3 and increased to a maximum of 0.48 for τ = 4. At τ = 4, $\alpha(\lambda)$ approached similar values compared to the spherical LAD. The increase in $\alpha(\lambda)$ from τ = 0 to 4 resulted in a ratio $\alpha_\mathrm{c}(\lambda)/\alpha_\mathrm{cf}$ of approximately 1.6 at 850 nm and 1.8 at 2200 nm wavelength (Fig. 4c). For θ_0 of 70° (Fig. 4 right column), the response of $\alpha(\lambda)$ on τ, is analog to the behavior found for the spherical LAD. The generally limited response of $\alpha(\lambda)$ on τ and LAD under large θ_0 is caused by the dominance of diffuse radiation, where the angular dependent extinction of direct radiation and reflectivity in the canopy is negligible.

For the planophile LAD, with mostly horizontally oriented leaves, the area of each leaf and the total probability of interaction with incoming radiation is largest compared to the spherical or even the erectophile distribution. The extinction coefficient k_ext for direct ration is approximated by a fixed value of 1, independent of θ_0 (see Table C1 and Fig. C1). Consequently, $\alpha(\lambda)$ is almost invariant with respect to θ_0 but also τ. For τ = 6, a maximum increase of $\alpha(\lambda)$ by 2 % at 700 nm wavelengths was determined.

https://doi.org/10.5194/egusphere-2024-3614
Preprint. Discussion started: 11 December 2024

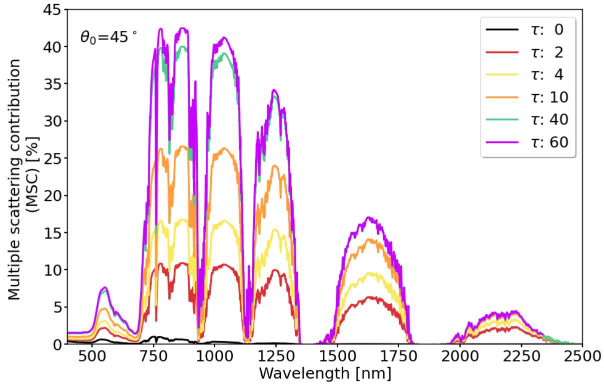

Figure 5. Relative contribution $\xi(\lambda)$ (in percent) of downward diffuse irradiance due to multiple scattering to the enhancement of spectral albedo $\alpha(\lambda)$. The calculations were performed with a non-reflecting surface ($\alpha(\lambda) = 0$) and a surface with an actual vegetation albedo. An intermediate solar zenith angle θ_0 of 45° was selected. Four cloud conditions were considered with cloud optical thickness τ (unitless) ranging between 0 and 60.

3.2 Contribution of multiple scattering to the enhancement of vegetation albedo

Multiple scattering between cloud base and the surface, here the TOC, is known to enhance the observed albedo (Weihs et al., 2001; Wendisch et al., 2004). The enhancement is caused by an additional contribution of radiation first reflected by the surface and then by the cloud base, contributing to $F^{\downarrow}_{\text{dif}}(\lambda)$. By definition, only $F^{\downarrow}_{\text{dif}}(\lambda)$ is affected by multiple scattering. The coupled models were used to determine the contribution of multiple scattering to the enhancement of $F^{\downarrow}_{\text{dif}}(\lambda)$ and $\alpha(\lambda)$. The contribution was estimated from the difference between $F^{\downarrow}(\lambda,\alpha(\lambda))$ from simulations accounting for $\alpha(\lambda)$ of vegetation and simulations of $F^{\downarrow}(\lambda,\alpha(\lambda) = 0)$ with no reflection from the surface. The simulations of $F^{\downarrow}(\lambda,\alpha(\lambda) = 0)$ were run with the same configuration as the previous simulations except for a fixed value of $\alpha(\lambda)$ = 0. The relative contribution $\xi(\lambda)$ of multiple-scattering is calculated by:

$$\xi(\lambda) = \frac{F^{\downarrow}(\lambda,\alpha(\lambda)) - F^{\downarrow}(\lambda,\alpha(\lambda) = 0)}{F^{\downarrow}(\lambda,\alpha(\lambda))}. \tag{8}$$

Figure 5 shows that $\xi(\lambda)$ is generally largest at wavelengths where $\alpha(\lambda)$ and $F^{\downarrow}(\lambda)$ are both highest and outside of the water vapor absorption bands. In cloud-free cases (τ = 0, black line) with scattering from molecules and aerosols only, $\xi(\lambda)$ is negligible with a maximum of about 1 % at 750 nm. With increasing values of τ, $\xi(\lambda)$ increased continuously over the entire spectra with a maximum between 750 to 900 nm wavelengths. For constant τ, $\xi(\lambda)$ decreases towards longer wavelengths as $F^{\downarrow}(\lambda)$ decreases too. For a value of τ = 60, a maximum $\xi(\lambda)$ of 42 % at 850 nm wavelength was determined. Increasing τ caused the cloud to reflect more of the upward radiation back down towards the TOC but at the same time the absolute $F^{\downarrow}(\lambda)$ decreases with increasing τ and thus the relative contribution of multiple scattering keeps increasing.

https://doi.org/10.5194/egusphere-2024-3614
Preprint. Discussion started: 11 December 2024

3.3 Broadband

3.3.1 Sensitivity of broadband top of canopy albedo on cloud optical thickness

Figure 6a, d, and g show α_{BB} as a function of τ for the spherical, erectophile, and planophile LADs, respectively. Reading Fig. 6a, d, and g along lines of constant θ_0 is interpreted as considering different cloud conditions at a fixed time on any given day. Independent of the LAD and for $\theta_0 \leq 60°$, the broadband α_{BB} increases with increasing τ. Within one LAD, the increase in α_{BB} is generally largest for θ_0 = 25°. The sensitivity of α_{BB} on τ reduces with increasing θ_0. Comparing the three LADs, the largest variability is found for the erectophile LAD followed by the spherical LAD. For θ = 25° the transition from cloud-free to overcast conditions (τ = 6) leads to an increase of α_{BB} by 0.1 for the erectophile LAD and an increase of 0.08 for the spherical LAD. In case of the planophile LAD, α_{BB} is almost insensitive to τ with an increases by about 0.002. For θ_0 > 60°, the response of α_{BB} is reversed for the spherical and the erectophile LAD, where α_{BB} decreases with increasing τ. Regardless of θ_0 and the LAD, α_{BB} tends to an asymptotic value of 0.23 when τ approaches a value of 4 as the radiation is dominated by diffuse radiation (e.g., see Fig. 3c,d) and becomes insensitive to changes in θ_0. Neglecting cloud–vegetation-radiation interactions, indicated by the dashed lines, leads to a general underestimation of α_{BB} that is of similar magnitude for all three LADs. The deviations generally increase with increasing τ.

3.3.2 Sensitivity of broadband top of canopy albedo on solar zenith angle and direct fraction

Figure 6b, e, and h show the dependence of α_{BB} on θ_0 for constant τ. The response of α_{BB} along the lines of constant τ represents the diurnal cycle of the Sun under constant cloud conditions. In the case of the spherical and erectophile LAD, an increase in θ_0 is associated with an increase in α_{BB}. The change in α_{BB} is largest for cloud-free conditions ($\tau = 0$), being most pronounced for the erectophile LAD, and followed by the spherical LAD. For τ = 0 the transition from θ_0 = 25° to θ_0 = 70° leads to an increase in α_{BB} by 0.12 for the erectophile LAD and an increase of 0.09 for the spherical LAD, which is similar in magnitude compared to the change of τ for constant θ_0 = 25. For increasing τ, the sensitivity of α_{BB} to θ_0 is progressively reduced until it becomes insensitive to θ_0 for τ = 6. As for the sensitivity of α_{BB} to τ, an overcast sky that is dominated by diffuse radiation, α_{BB} becomes insensitive to the angular dependent extinction of the radiation in the canopy, and thus the Sun's diurnal cycle becomes less influential on α_{BB}. In the case of the planophile LAD, α_{BB} is almost insensitive to θ_0 independent of τ.

Figure 6c, f, and i show the relationship of α_{BB} on $f_{\mathrm{dir}}(\lambda)$, which is comprised of the interplay between τ and θ_0. Plotting $f_{\mathrm{dir}}(\lambda)$ instead of τ removes the exponential relationship in Eq. 6 and leads to a linear response. For the spherical and erectophile LAD, and θ_0 less than 60°, α_{BB} increase with decreasing $f_{\mathrm{dir}}(\lambda)$, while for larger values of θ_0 the opposite is true. This is in accordance with the response of α_{BB} on τ (see Fig. 6a, d, and g). Along lines of constant $f_{\mathrm{dir}}(\lambda)$ the maximum sensitivity for the spherical and erectophile LAD is found for the cloud-free case. For same LAD, the maximum sensitivity for constant θ_0 is associated with the Sun almost in the zenith (θ = 25°). For the smallest values of $f_{\mathrm{dir}}(\lambda)$, i.e., where diffuse radiation dominates, the linear relationship between α_{BB} and $f_{\mathrm{dir}}(\lambda)$ is absent. These deviations are not caused by a change in $f_{\mathrm{dir}}(\lambda)$

https://doi.org/10.5194/egusphere-2024-3614
Preprint. Discussion started: 11 December 2024

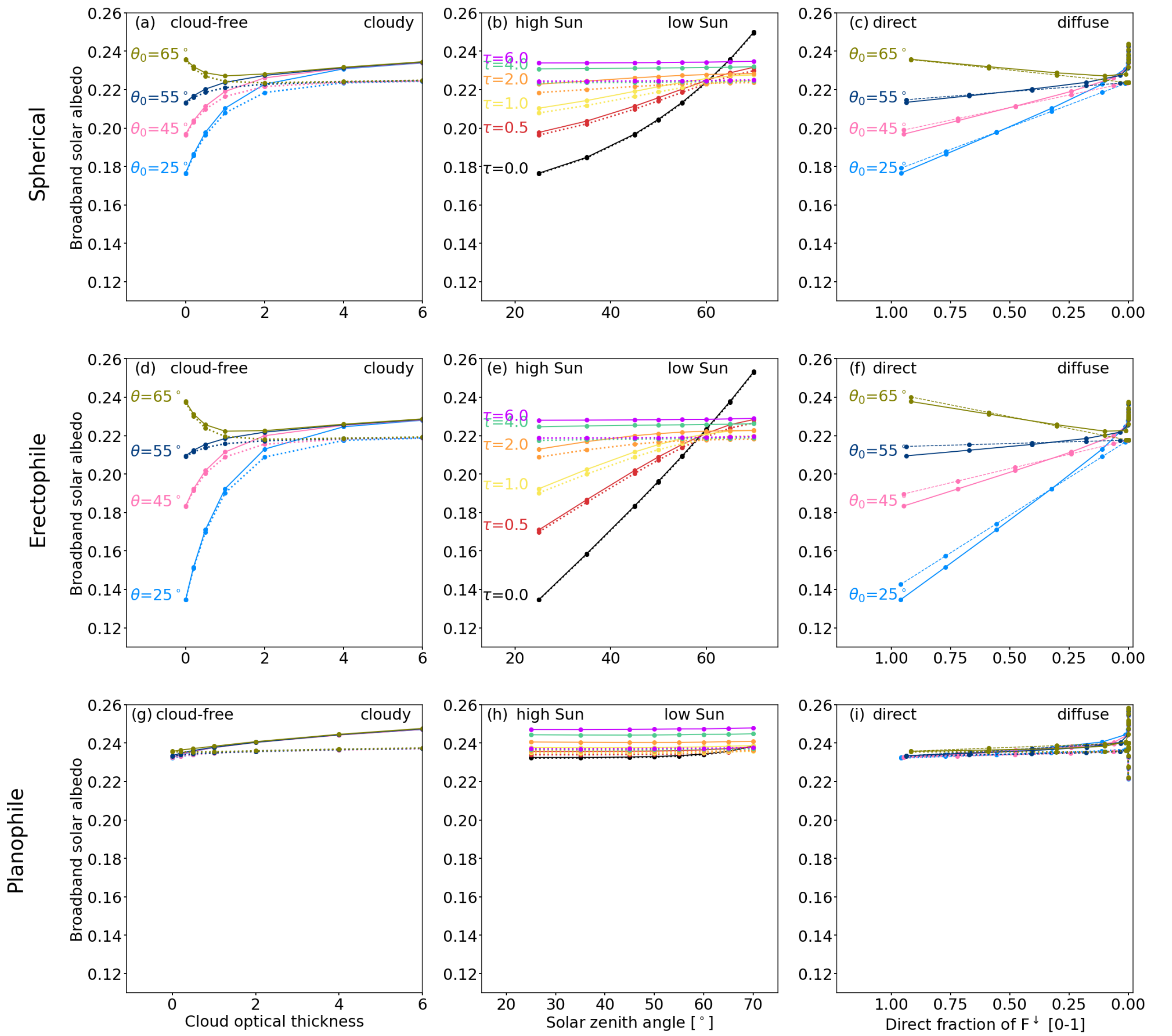

Figure 6. First column: Broadband, solar albedo $\alpha_{\mathrm{BB,sol}}$ as a function of cloud optical thickness τ. Second column: $\alpha_{\mathrm{BB,sol}}$ as a function of solar zenith angle θ_0. Third column: $\alpha_{\mathrm{BB,sol}}$ as a function of the direct fraction $f_{\mathrm{dir}}(\lambda)$ of the downward irradiance $F^{\downarrow}$. Lines along θ_0 and τ are color-coded and indicated directly next to the lines of α_{BB}. Columns from top to bottom provide α_{BB} based on the spherical, the erectophile, and the planophile leaf angle distribution, respectively. The dashed lines in the first and second column represent α_{BB} obtained for uncoupled simulations that neglect cloud–vegetation-radiation interactions. The dashed lines in the third column represent parameterized α_{BB}.

https://doi.org/10.5194/egusphere-2024-3614
Preprint. Discussion started: 11 December 2024

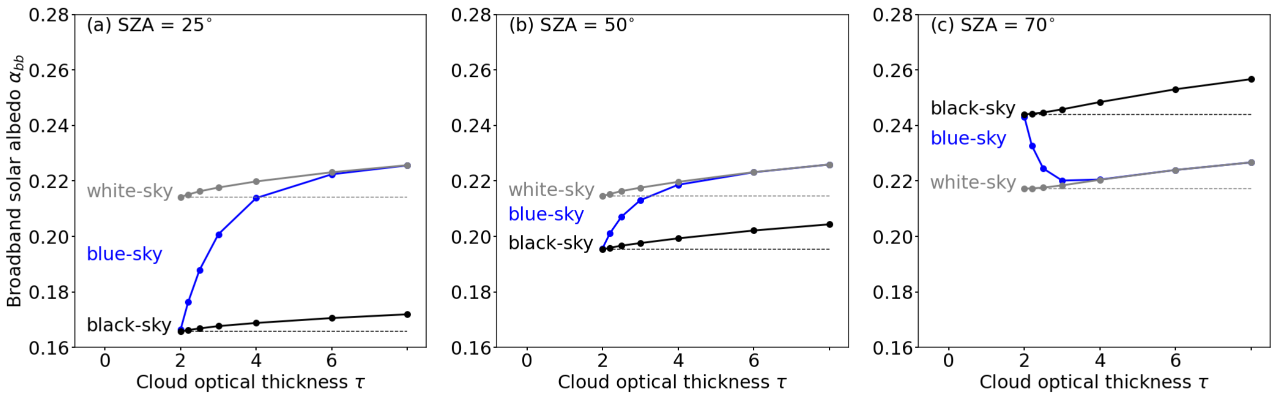

Figure 7. (a–c) Broadband, solar albedo α_{BB} as a function of cloud optical thickness τ for three solar zenith angles θ_0 of 25, 50, and 70°, respectively. Simulations are performed for a spherical leaf angle distribution and a leaf area index of 3 $\mathrm{m}^2\ \mathrm{m}^{-2}$. Simulations including the direct and diffuse fraction of $F^{\downarrow}$ (blue-sky albedo) are given in blue. Simulations including only the direct fraction of $F^{\downarrow}$ (black-sky albedo) are given in black, while broadband albedo including only the diffuse fraction of $F^{\downarrow}$ (white-sky albedo) are given in gray. The dashed lines provide a reference for black-sky and blue-sky albedo.

but a related to the shift in the spectral weighting of $\alpha(\lambda)$ by $F^{\downarrow}(\lambda)$. The planophile LAD is generally insensitive to to changes in $f_{\mathrm{dir}}(\lambda)$ irrespective of θ_0.

3.3.3 Separating the influence of the direct and diffuse fraction from the wavelength shift in the downward irradiance

With $f_{\mathrm{dir}}(\lambda)$ the main parameter controlling α_{BB}, the individual contributions of the direct and diffuse $F^{\downarrow}(\lambda)$ to change in α_{BB} were quantified by simulating hypothetical cases with either the direct or diffuse component of $F^{\downarrow}(\lambda)$. The albedo that includes only direct radiation is commonly referred to as the black-sky albedo, while the albedo that includes only diffuse radiation is referred to as the white-sky albedo. Black-sky and white-sky albedo are extreme cases and the actual albedo observed in nature is called blue-sky albedo, which is an interpolation between the two extreme cases (Lucht et al., 2000). Figures 7a–c show the broadband solar albedo as a function of τ for the spherical LAD and three values of θ_0 with 25°, 50°, and 70°, respectively. In each panel, the given blue-sky albedo is identical with the graphs given in Fig. 6a. For values of θ_0 of 25° and 50°, α_{BB} is lowest for the black-sky albedo, while the highest values of α_{BB} are found for the white-sky albedo. The black-sky and white-sky albedo increase with increasing τ. The blue-sky albedo, as an interpolation between the black-sky and white-sky albedo, is closest to the black-sky albedo for cloud-free conditions and approaches the white-sky albedo under overcast conditions ($\tau > 6$). The different slopes of the blue-sky albedo for different values of θ_0 are caused by the different penetration depth of the direct radiation into the canopy and therefore the angular reflectivity of the surface approximated by the parameterization of $k_{\mathrm{ext}}(\theta)$ (see Section C). It is further shown that with increasing θ_0 black-sky and white-sky become similar up to a point where the black-sky albedo exceeds the white-sky albedo. For an example case of θ_0 of 70°, increasing τ results in a decrease of the blue-sky albedo.

https://doi.org/10.5194/egusphere-2024-3614
Preprint. Discussion started: 11 December 2024

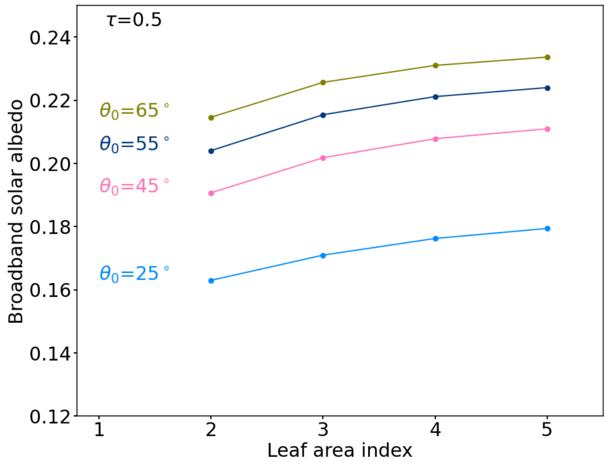

Figure 8. Above canopy broadband solar albedo α_{bb} as a function leaf area index for an erectophile leaf angle distribution, solar zenith angles θ_0 between 25° and 65°, and a cloud optical thickness τ of 0.5.

The broadband α_{BB} is also altered by spectrally dependent scattering and absorption by clouds. The effects of the weighting shift are shown for the black-sky and white-sky albedo with respect to the cloud-free state with $\tau = 0$ (dashed lines as reference). For a value of θ_0 of 25°, the black-sky albedo increased by 0.005 and the white-sky albedo increased by 0.06 at $\tau = 8$ compared to the reference at $\tau = 0$. For a value of θ_0 of 70°, the black-sky albedo increased by 0.06 and the white-sky albedo increased by 0.07 at $\tau = 8$ compared to the reference at $\tau = 0$. Regardless of θ_0, the contributions of the wavelength shift to black-sky, white-sky, and blue-sky albedo enhance α_{BB}, but are relatively small compared to the overall increase in blue-sky albedo caused by the change in $f_{\mathrm{dir}}(\lambda)$. The relatively small effect is due to the generally low values of $\alpha(\lambda)$ of vegetation below 700 nm wavelength, where $F^{\downarrow}(\lambda)$ is highest and vice versa. However, it should be noted that the relative contribution and importance of the wavelength shift increases with τ as the absolute difference between the black-sky and white-sky albedo becomes smaller with increasing θ_0 (see Fig. 7d–f). Furthermore, the wavelength shift continues to contribute to a changing α_{BB}, while the contribution of a changing $f_{\mathrm{dir}}(\lambda)$ is irrelevant beyond $\tau = 6$ (see Fig. B in the Appendix).

3.3.4 Sensitivity of broadband top of canopy albedo on the leaf area index

The previous simulations used the SCOPE2.0 default value of 3 for the LAI. Simulations for LAI values from 2 to 5 were performed for all three LADs to account for changes in the LAI, e.g., due to the annual vegetation cycle or leaf loss due to drought. Furthermore, LAI values within this range are expected to show the largest effects on $F^{\uparrow}(\lambda)$ and α_{BB} as reflectances start to saturate for LAI values larger than 5 (Houborg and Boegh, 2008). The non-linearity between LAI and reflected radiation results from an increasing overlap of leaves with increasing LAI. Therefore, the additional leaf area contributing to scattering and abortion does not continuously increase. In a first approximation the relationship between LAI and extinction of radiation in the canopy is commonly described by an exponential function that depends on the vegetation extinction coefficient $k_{\mathrm{ext}}(\theta, \lambda)$.

https://doi.org/10.5194/egusphere-2024-3614
Preprint. Discussion started: 11 December 2024

The vegetation extinction factor $k_{\mathrm{ext}}(\theta, \lambda)$ itself also depends on wavelength, direct and diffuse fraction of incident radiation, LAD, and the incident angle θ (Bréda, 2003). A brief overview of the effect of different LAI, LAD, and θ on the extinction of radiation in the canopy is given in Section C in the Appendix.

Variations in the LAI affected $\alpha(\lambda)$ over the entire wavelength range from 400 to 2400 nm. Increasing LAI resulted in higher values of $\alpha(\lambda)$ at TOC for wavelengths greater than 700 nm, as vegetation typically has higher albedo values compared to bare soil in this wavelength range. Conversely, for wavelengths less than 700 nm, an increase in LAI resulted in a decrease in $\alpha(\lambda)$ at TOC because the albedo of vegetation is lower than the albedo of bare, dry soil (Yang et al., 2021). Figure 8 shows α_{BB} as a function of LAI for the spherical LAD and a value of τ of 0.5. It shows that α_{BB} increases with increasing LAI due to the dominant increase in $\alpha(\lambda)$ at wavelengths greater than 700 nm wavelengths compared to the reduction in $\alpha(\lambda)$ at shorter wavelengths. The sensitivity α_{BB} on LAI is similar for all simulated θ_0. The nonlinearity between α_{BB} and τ is caused by the exponential contribution in Eq. 6. In addition, the contribution to α_{BB} by enhanced reflection from vegetation greater than 700 nm wavelengths overweight the decreased reflection from vegetation from shorter wavelengths. Compared to the spherical LAD that is shown in Fig. 8, the lines of constant θ_0 are spread further apart for the erectophile and are almost overlapping for the planophile LAD (not shown here). This is due to the greater sensitivity of the erectophile LAD and the reduced sensitivity of the planophile LAD to θ_0 compared to the spherical LAD (see Fig. 6 center column).

3.3.5 Effect of neglected cloud effect on vegetation on radiative budget and parameterization of cloud effect on broadband surface albedo

The analysis showed that α_{BB} varied by up to 0.12 between cloud-free (τ = 0) and cloudy conditions (τ = 6) for the erectophile LAD and a value of θ_0 of 25° (Fig. 6e). The cloud-induced changes in α_{BB} therefore affect the surface radiative energy budget. It is therefore necessary to analyze the deviations in the surface radiation budget when cloud–vegetation-radiation interactions are neglected. The effect is quantified by the solar radiative forcing ΔF at the canopy level between simulations with a fixed cloud-free albedo and an albedo that accounts for cloud–vegetation-radiation interactions. The forcing ΔF is calculated with:

$$\Delta F = (F^{\downarrow}_{\mathrm{BB}} - \alpha_{\mathrm{BB,c}} \cdot F^{\downarrow}_{\mathrm{BB}}) - (F^{\downarrow}_{\mathrm{BB}} - \alpha_{\mathrm{BB,cf}} \cdot F^{\downarrow}_{\mathrm{BB}}), \qquad (9)$$

where $F^{\downarrow}_{\mathrm{BB}}$ is the TOC downward irradiance, $\alpha_{\mathrm{BB,cf}}$ the albedo under cloud-free conditions (i.e., τ = 0), and $\alpha_{\mathrm{BB,c}}$ the albedo under the influence of clouds. Equation 9 simplifies to:

$$\Delta F = F^{\downarrow}_{\mathrm{BB}} \cdot (\alpha_{\mathrm{BB,cf}} - \alpha_{\mathrm{BB}}), \qquad (10)$$

where ΔF becomes negative, when the albedo α_{BB} is greater than the albedo under cloud-free conditions and vice versa.

Figure 9a and b show ΔF plotted as a function of τ, θ, and for the spherical and erectophile LAD, respectively. In general, ΔF is most sensitive to the smallest values of τ, regardless of the actual value of θ_0, due to the sensitivity of α_{BB} to small τ. For θ_0 less than 60°, the increase in α_{BB} with τ results in more radiation being reflected by the canopy compared to a fixed canopy albedo, resulting in a negative value of ΔF. The largest negative value of $\Delta F \approx -40\,\mathrm{W\ m^{-2}}$ occurs for the combination of θ = 25° and τ = 4. For θ = 50° and τ = 2, a maximum ΔF of $-12\,\mathrm{W\ m^{-2}}$ is reached. For values of θ_0 greater than 60°,

https://doi.org/10.5194/egusphere-2024-3614
Preprint. Discussion started: 11 December 2024

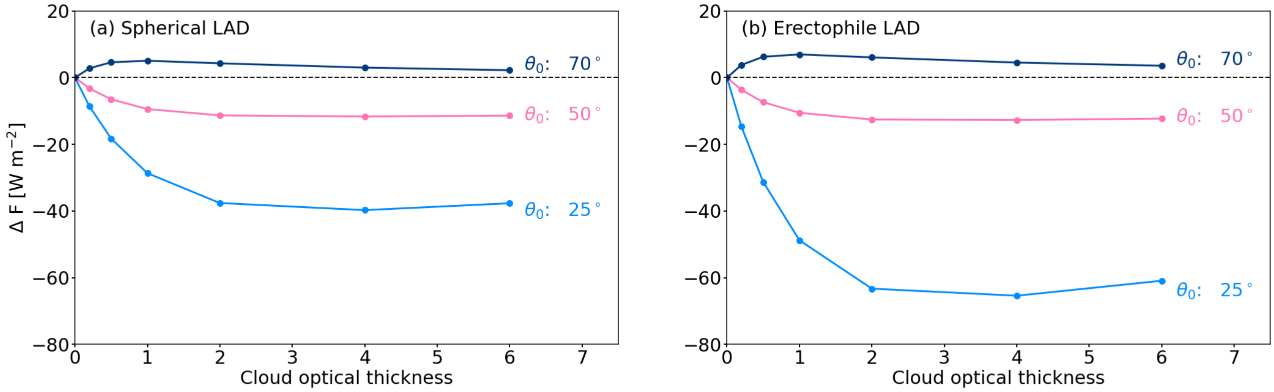

Figure 9. Absolute difference in above canopy broadband solar radiative forcing $\Delta F_{\mathrm{BB,sol}}$ due to the cloud-modulated canopy albedo for the spherical **(a)** and erectophile **(b)** leaf angle distribution. $\Delta F_{\mathrm{BB,sol}}$ is given as a function of cloud optical thickness τ for three solar zenith angle θ_0 of 25°, 50°, and 70°.

α_{BB} becomes smaller with increasing τ, leading to positive values of ΔF. Positive ΔF are associated with higher absorption of radiation by the canopy. For θ_0 = 70°, ΔF increases with τ to a maximum value of about 5 W m^{-2}. For the erectophile LAD, ΔF is subject to larger variations between extreme values of −60 W m^{-2} (θ = 25°) and 10 W m^{-2} (θ = 70°). In contrast, variations in τ concerning the planophile LAD, lead to negligible effects on ΔF with maximum values of 3 W m^{-2} (not shown here). At the level of individual LADs, the varied parameters τ and θ_0 are equally relevant on ΔF. Consequently, the inclusion of cloud–vegetation-radiation interactions is most relevant for canopies with an erectophile LAD and the spherical LAD.

3.3.6 Parameterization of cloud–vegetation-radiation effects

We propose a parameterization of α_{BB} as a function of $f_{\mathrm{dir}}(\lambda)$ to account for the cloud-vegetation-radiation interactions that occur during the transition from cloud-free to cloudy conditions (Fig. 6). The parameterization takes as input the atmospheric parameters θ_0 and $f_{\mathrm{dir}}(\lambda)$, and the vegetation parameter LAI and LAD. Spherical, erectophile, and planophile LAD are considered in the parameterization. The parameterization of α_{BB} is formalized by:

$$\alpha_{\mathrm{BB}} = g(\mu) \cdot f_{\mathrm{dir}}(\lambda) + b_1 \cdot LAI^2 + b_2 \cdot LAI + b_3 \tag{11}$$

where $\mu = \cos(\theta_0)$ and $g(\mu)$ is given by:

$$g(\mu) = a_1 \cdot \mu^3 + a_2 \cdot \mu^2 + a_3 \cdot \mu + a_4. \tag{12}$$

The parameters a_1 to a_4 and b_1 to b_3 for the spherical, erectophile, and planophile LAD are provided in Table 3.

The parameterization of α_{BB} has been evaluated against the simulated values of α_{BB} and is overlaid in the right column of Fig. 6. The values of α_{BB} from the simulations and the parameterization mostly overlap, indicating a good agreement of the parameterization with the simulations. Regardless of the LAD, discrepancies appear mainly when $f_{\mathrm{dir}}(\lambda)$ approaches a value

https://doi.org/10.5194/egusphere-2024-3614
Preprint. Discussion started: 11 December 2024

Table 3. Parameters and polynomials for the parameterized broadband solar albedo α_{BB}. Maximal deviations $\Delta\alpha_{\mathrm{BB}}$ between simulation and parameterization.

Leaf angle distribution	a_1	a_2	a_3	a_4	b_1	b_2	b_3	$\Delta\alpha_{\mathrm{BB}}$
spherical	−0.0490	0.1722	−0.2839	0.1059	−0.0024	0.0238	0.1739	0.003
erectophile	−0.2310	0.3587	−0.3694	0.1340	−0.0021	0.0212	0.1729	0.008
planophile	−0.0633	0.1483	−0.1166	0.0229	−0.0024	0.0236	0.1909	0.002

of 0. General differences appear for the erectophile LAD, but remain below a value of $\Delta\alpha_{\mathrm{BB}}$ = 0.005, which corresponds to a relative error of 2.3% with respect to α_{BB} = 0.22. A shortcoming of the proposed parameterization is that it only incudes the contribution of the change in the direct and diffuse fraction on α_{BB}, as it does not include the shift in the spectral weighting, which persists beyond τ = 6 when $f_{\mathrm{dir}}(\lambda)$ = 0. However, the contribution of the wavelength shift is generally small compared to the effect of $f_{\mathrm{dir}}(\lambda)$ (see Fig. 7 and Section B). A caveat of the parametrization is the limited wavelength range spanning only from 0.4 to 2.4 µm, and that dependencies on the biochemical composition, e.g., chlorophyll content or leaf structure, of the canopy are not included.

4 Summary and conclusions

This study investigated cloud–vegetation-radiation interactions by coupling an atmospheric radiative transfer model (RTM), the library for radiative transfer (libRadtran), and a vegetation RTM, the Soil Canopy Observation of Photosynthesis and Energy fluxes (SCOPE2.0). This goes beyond previous model set-ups, where vegetation RTMs neglected the influence of clouds, which are now explicitly included in the coupled radiative transfer simulations.

The coupled simulations were performed for the inclusive interval of solar zenith angles θ_0 between 25° and 70°. A stratiform liquid water cloud was simulated with cloud optical thickness τ ranging from 0, for cloud-free conditions, to 80, for fully overcast conditions. The diversity of plant characteristics was attempted to be represented by spherical, erectophile, and planophile leaf angle distributions (LADs), and variations of the leaf area index (LAI) between 2 and 5 $\mathrm{m^2\,m^{-2}}$ (inclusive). The simulations by libRadtran and SCOPE2.0 covered a wavelength range from 0.4 to 2.4 µm. The iterative coupling was realized by initializing SCOPE2.0 with the spectral, downward direct $F^{\downarrow}_{\mathrm{dir}}(\lambda)$ and diffuse irradiance $F^{\downarrow}_{\mathrm{dif}}(\lambda)$ provided by libRadtran. libRadtran was initialized with a first guess vegetation albedo, which was replaced in the next iteration step with the vegetation albedo provided by SCOPE2.0. Two cycles were found to be sufficient for the iteration to converge.

The absolute change in spectral albedo $\alpha(\lambda)$ between uncoupled and coupled simulations was around 10 to 15 %. Differences particularly occurred outside the water vapor absorption bands and where high values of $\alpha(\lambda)$ and $F^{\downarrow}(\lambda)$ coincide. The iterative coupling was found to be particularly important to account for multiple scattering between the top of canopy and the cloud base. The relative contribution of multiples scattering to the enhancement of α_{BB} continuously increases with increasing τ. The LAI was found to have the largest impact on the resulting spectral and broadband α, which agrees with other existing literature,

https://doi.org/10.5194/egusphere-2024-3614
Preprint. Discussion started: 11 December 2024

e.g., Jones and Vaughan (2010). Considering constant LAI, the largest sensitivity and absolute difference in α_{BB} were found for the erectophile LAD, especially for combinations of small τ < 6 and small θ_0 < 50°, i.e., large values of direct fraction $f_{\mathrm{dir}}(\lambda)$. It showed that the direct fraction could explain the difference between spectral and broadband α between cloud-free and cloudy conditions. Generally lower sensitivities of spectral and broadband α on τ and θ_0 were found for the spherical LAD, while the effect of both was negligible for the planophile LAD. The sensitivity of $\alpha(\lambda)$ on LAI, LAD, and θ_0 decreased continuously with decreasing fraction $f_{\mathrm{dir}}(\lambda)$. This is caused by the dominating fraction of isotropically reflected radiation from the surface that is less sensitive on the incident angle of the radiation compared to the reflection of direct radiation. The second effect that influenced spectrally integrated broadband albedo α_{BB} was the wavelength dependent absorption and scattering by clouds, which shifted the weight of the incoming radiation towards shorter wavelengths. Due to the generally low values of $\alpha(\lambda)$ below 700 nm, the effect of the wavelength shift was found to be small in absolute values, enhancing α_{BB} by up to 0.07 (θ_0 = 70° and τ = 6). Relatively speaking, the contribution of the wavelength shift increased with increasing τ. In conclusion, the change in $f_{\mathrm{dir}}(\lambda)$ is relevant for values of τ between 0 and 6, while the shift in the spectrla weighting of $\alpha(\lambda)$ with $F^{\downarrow}(\lambda)$ is relevant for values of τ beyond 6.

The radiative effect of clouds on α_{BB} and the resulting radiation budget below clouds was estimated in terms of the radiative forcing ΔF at top of canopy. The radiative forcing ΔF was determined between simulations that neglected and included clouds. The greatest sensitivity of ΔF was found for the transition from cloud-free to cloudy conditions (τ < 2). The largest absolute values of ΔF were identified for θ_0 =25°, leading to negative ΔF of up to -60 W m^{-2}, implying a stronger reflection by vegetation in the coupled simulations compared to uncoupled simulations that neglected the influence of clouds. The maximal values of ΔF decreased with increasing θ_0 and also turned the sign, so that for θ = 70°, ΔF became positive, with values up to 8 W m^{-2}.

The nearly linear correlation between α_{BB} and $f_{\mathrm{dir}}(\lambda)$ has been exploited to parameterize the effect of clouds on α_{BB} over vegetated areas. The parameterization considers for θ, LAI, LAD, and $f_{\mathrm{dir}}(\lambda)$. It was demonstrated that the parameterization is capable of representing the simulated cloud–vegetation-radiation interactions with a relative error that is less than 2.4 %. The approach to parameterize the effect of clouds on α_{BB} over vegetated areas may be suitable for implementation in numerical weather prediction or global climate models to improve the surface radiation budget over vegetated areas under cloudy conditions. However, the current parameterization is limited to the wavelength range from 0.4 to 2.4 µm, which has to be overcome by extending the simulated wavelength range. The current version also does not consider for the dependencies on the biochemical composition, e.g., chlorophyll content or leaf structure.

Appendix A: Influence of clouds on downward irradiance

Radiation passing through the atmosphere is scattered and absorbed by aerosol particles, gas molecules, and clouds. The influence of clouds on the direct irradiance $F^{\downarrow}_{\mathrm{dir}}(\lambda)$ and the diffuse irradiance $F^{\downarrow}_{\mathrm{dif}}(\lambda)$ components of the total irradiance $F^{\downarrow}(\lambda)$ is shown in Fig. A1 for an intermediate solar zenith angle θ_0 of 45°. All spectra are characterized by water-vapor absorption bands at 933–946 nm, 1118–1144 nm, 1350–1480 nm, and 1810–1959 nm wavelengths due to molecular absorption. An

https://doi.org/10.5194/egusphere-2024-3614
Preprint. Discussion started: 11 December 2024

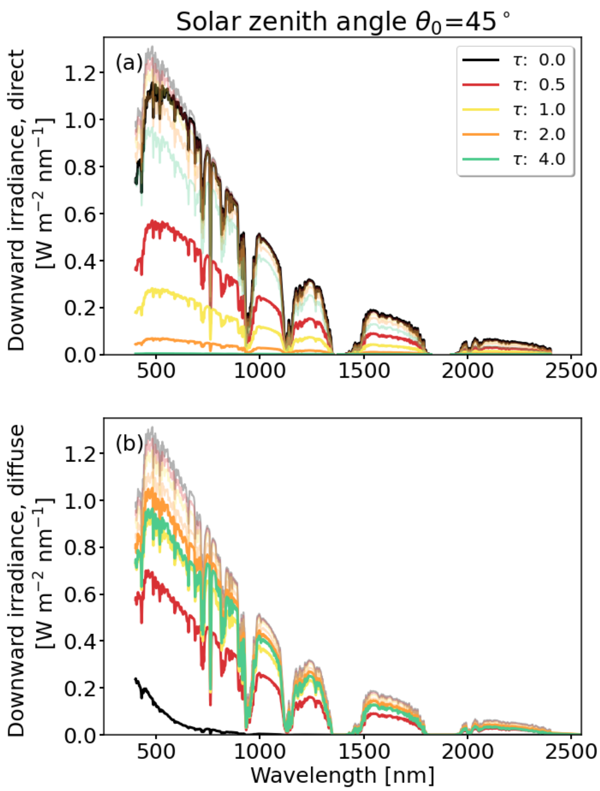

Figure A1. Panel **(a)** and **(b)** show spectral, downward, direct $F^{\downarrow}_{\mathrm{dir}}(\lambda)$ and diffuse $F^{\downarrow}_{\mathrm{dif}}(\lambda)$ irradiance, respectively. In both panels spectral, downward, total irradiance $F^{\downarrow}(\lambda)$ is underlaid by faded colors. Cloud optical thickness τ is indicated by the colored lines. Simulations based on a spherical leaf angle distribution for a solar zenith angle θ_0 = 45°.

increase in τ results in a decrease in $F^{\downarrow}_{\mathrm{dir}}(\lambda)$ (Fig. A1a). Wavelengths below 900 nm that are outside of the absorption bands are primarily affected by Rayleigh and Mie scattering (Mie, 1908), leading to a flattening of the spectrum below 500 nm. Wavelengths above 900 nm and within the water–vapor-absorption bands are dominated by absorption. It is further noted that with decreasing / increasing θ_0 the path of the radiation thought the atmosphere and the cloud becomes shorter / longer, leading to less / more scattering processes. Consequently, the same values of cloud optical thickness τ yield $F^{\downarrow}_{\mathrm{dir}}(\lambda)$ that are greater / lesser for θ_0 lesser / greater than θ_0 = 45°. Radiation scattered at least once by atmospheric constituents is removed from the direct component $F^{\downarrow}_{\mathrm{dir}}(\lambda)$ and contributes to the diffuse component $F^{\downarrow}_{\mathrm{dif}}(\lambda)$ given in Fig. A1b. For the cloud-free case (black), $F^{\downarrow}_{\mathrm{dif}}(\lambda)$ is close to zero except for wavelengths λ < 750 nm due to Rayleigh scattering. Regardless of θ_0, including clouds in the simulations leads to an overall increase in $F^{\downarrow}_{\mathrm{dif}}(\lambda)$. However, the increase is not continuous and reaches maximum values for τ between 2 and 4 at θ_0 = 25° and τ around 1 at θ_0 = 75°. This is a result of the pronounced forward peak in the scattering phase function of water droplets, which enhances scattering toward the surface compared to cloud-free conditions. According to Bohren (1987), the maximum $F^{\downarrow}_{\mathrm{dif}}(\lambda)$ occurs under cloudy conditions when $\tau \approx \ln(2/(1-g)) \cdot \cos(\theta_0) \approx 2.6$, with $g = 0.85$

https://doi.org/10.5194/egusphere-2024-3614
Preprint. Discussion started: 11 December 2024

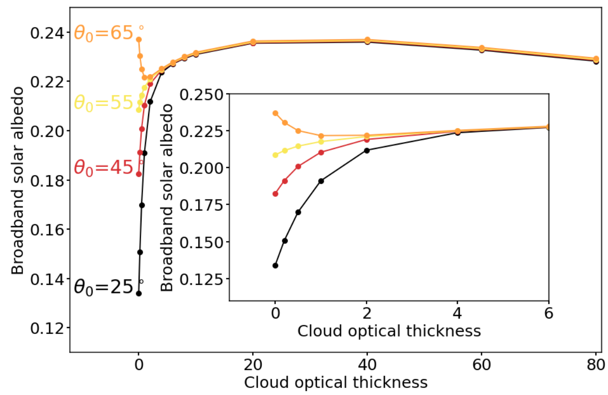

Figure B1. Above canopy broadband solar albedo α_{bb} as a function of cloud optical thickness τ ranging from 0 to 80 and for four solar zenith angles, with a default leaf area index of 3. An erectophile leaf angle distribution is assumed.

the asymmetry factor with a representative value for clouds in the visible-near infrared wavelength range (Irvine and Pollack, 1968).

Appendix B: Sensitivity of broadband solar albedo on the full range of cloud optical thickness

Coupled simulations of spectral irradiance $F(\lambda)$ and albedo $\alpha(\lambda)$ have been performed for cloud optical thickness τ with values between 0 and 80. Integration of $\alpha(\lambda)$ using Eq. 4 results in the broadband α_{BB} weighted by the incoming $F^{\downarrow}(\lambda)$. Spectral dependent scattering and absorption by clouds shifts the relative weighting towards shorter wavelengths. Figure B1 shows the response of α_{BB} on τ for the erectophile leaf angle distribution (LAD). Initially, α_{BB} increases or decreases with increasing τ until the diffuse component of $F^{\downarrow}(\lambda)$ dominates at τ = 6. This increase is related to the transition from only direct (τ = 0) to diffuse (τ = 6) downward irradiance $F^{\downarrow}(\lambda)$. Beyond a value of τ = 6, the further increase of α_{BB} is only related to the shift of the weighting in $F^{\downarrow}(\lambda)$ to shorter wavelengths. The spectral slope of the incoming radiation - roughly decreasing with increasing wavelength - and the spectral slope of the vegetation - low $\alpha(\lambda)$ below 700 nm, steep increase, and decreasing with increasing wavelength - lead to a maxima in the convolution of $\alpha(\lambda)$ and $F^{\downarrow}(\lambda)$, such that α_{BB} becomes maximal at $\tau \approx$ 20. Beyond this optimum, α_{BB} decreases because the spectral weighting in $F^{\downarrow}(\lambda)$ is shifted more and more into the spectral range where the radiation is almost completely absorbed by vegetation. The simulation with the erectophile LAD represents an extreme case. For the spherical and the planophile LAD, a reduced sensitivity of α_{BB} to τ between 0 and 6 was found. However, the position of the maximum at around τ = 20 showed to be insensitive to the selected LAD.

Appendix C: Approximate direct beam extinction in vegetation

Within a homogeneous vegetation layer, the radiative transfer can be approximated by the turbid medium approach (Jones and Vaughan, 2010). The attenuation of direct radiance $I_0(\lambda)$ at the penetration depth z can be expressed by the Equation 6.

https://doi.org/10.5194/egusphere-2024-3614
Preprint. Discussion started: 11 December 2024

Table C1. Vegetation extinction coefficients $k_{\text{ext}}(\theta)$ for the spherical, planophile, and erectophile leaf angle distribution taken from Jones and Vaughan (2010).

Distribution	Approximation of $k_{\text{ext}}(\theta)$
spherical	$k = 1/(2 \cdot \cos\theta)$
erectophile	$k = (2 \cdot \tan\theta)/\pi$
planophile	$k = 1$

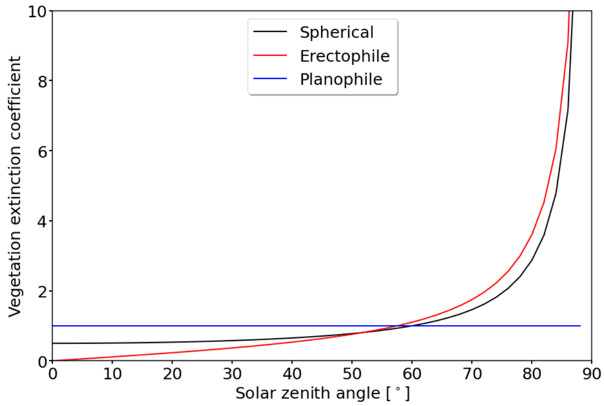

Figure C1. Extinction coefficient in dependence of incident angle θ for the spherical, erectophile, and planophile leaf angle distribution.

Among other factors, the vegetation extinction coefficient $k_{\text{ext}}(\theta, \lambda)$ depends on the stand structure and canopy architecture, wavelength, direct and diffuse fraction of incident radiation, and the incident angle θ (Bréda, 2003). It is therefore not straight forward to determine analytical expressions for $k_{\text{ext}}(\theta, \lambda)$ (Bréda, 2003; Jones and Vaughan, 2010). First order approximations are provided, which do neglect the wavelength dependence of $k_{\text{ext}}(\theta, \lambda)$. It is also assumed that the solar zenith angle θ_0 is equal to the incident angle θ. However, state of the art vegetation radiative transfer models (RTMs) such as SCOPE2.0 account for wavelength dependent effects by using numerical procedures (Yang et al., 2021). In the literature various values of $k_{\text{ext}}(\theta)$ exist, ranging from fixed values (Pierce and Running, 1988; Wan et al., 2021); over empirical, tabulated values (Bréda, 2003); to trigonometric functions that account for the dependence on the incident angle of radiation (Jones and Vaughan, 2010). Figure C1 shows $k_{\text{ext}}(\theta)$ as a function of θ for the spherical, erectophile, and planophile LAD. The planophile leaf angle distribution (LAD) is approximated with a value of $k_{\text{ext}}(\theta) = 1$. The spherical and erectophile LAD are described by the trigonometric functions given in Table C1. For $\theta < 52°$, $k_{\text{ext}}(\theta)$ of the spherical LAD exceeds $k_{\text{ext}}(\theta)$ of the erectophile LAD. The erectophile LAD is characterized by a steeper slope and, therefore, $k_{\text{ext}}(\theta)$ of the erectophile LAD is more sensitive to changes on θ. For $\theta > 52°$, $k_{\text{ext}}(\theta)$ of the erectophile LAD exceed the spherical LAD resulting in a larger $k_{\text{ext}}(\theta)$ with increasing θ. Note that extinction includes the processes of scattering and absorption, which means that an increase in $k_{\text{ext}}(\theta)$ means an increase in absorption in the canopy, but can also be caused by an increase in scattering.

https://doi.org/10.5194/egusphere-2024-3614
Preprint. Discussion started: 11 December 2024

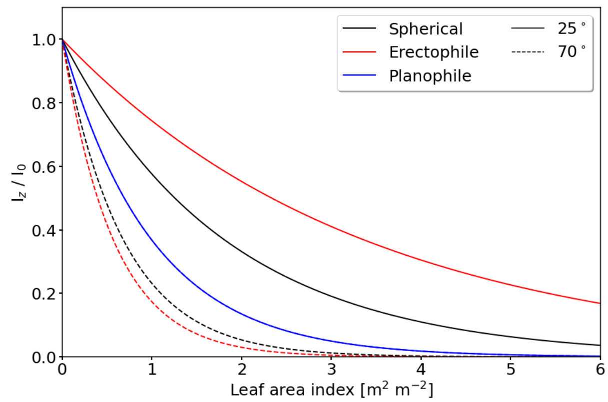

Figure C2. Ratio I_z/I_0 of direct radiance I_z at penetration depth z=LAI calculated with Eq. 6 and direct beam radiance I_0 at top of canopy as a function of leaf area index LAI. Two incident angles θ of 25° and 70° are given.

The estimated values of $k_{\text{ext}}(\theta)$ are used to estimate the extinction of direct radiance in dependence of the LAI. Figure C2 shows that for the Sun near the zenith (θ = 25°) the slope is steepest for the planophile LAD, followed by the spherical and erectophile LAD. The incident direct radiation is reduced to 50 % (I_z/I_0 = 0.5), when LAI values of 0.7, 2.3, and 1.26 for the planophile, spherical, and erectophile LADs are exceeded, respectively. For the Sun near the horizon (θ = 70°) the slope is steepest for the erectophile LAD, followed by the spherical and planophile LAD. The ratio I_z/I_0 = 0.5 is reached at LAI of 0.7, 0.4, and 0.5 for the planophile, erectophile, and septically LAD, respectively. As a result, for the default LAI of 3 and θ_0 = 70° the direct radiation cannot penetrate deep into the canopy, while for same LAI and θ_0 = 25° the direct radiation can penetrate deepest into the canopy for the erectophile, followed by the spherical and the planophile LAD.

Author contributions. **KW** designed and implemented the model coupling, performed the simulations, and drafted the manuscript. **EJ**, **AE**, **MS**, and **MW** contributed equally to the preparation of the manuscript. **AHu**, **HF**, and **AW** helped with the model set up and the revision of the manuscript.

Competing interests. The authors declare no competing interest.

Acknowledgements. We thank the German Centre for Integrative Biodiversity Research (iDiv) Halle-Jena-Leipzig, which is a research centre of the Deutsche Forschungsgemeinschaft (DFG). We also thank the Saxon State Ministry for Science, Culture and Tourism (SMWK) for funding thought grant 3-7304/44/4-2023/8846.

https://doi.org/10.5194/egusphere-2024-3614
Preprint. Discussion started: 11 December 2024

References

Aebi, C., Gröbner, J., Kazadzis, S., Vuilleumier, L., Gkikas, A., and Kämpfer, N.: Estimation of cloud optical thickness, single scattering albedo and effective droplet radius using a shortwave radiative closure study in Payerne, Atmos. Meas. Tech., 13, 907–923, https://doi.org/10.5194/amt-13-907-2020, 2020.

Anderson, G. P., Clough, S. A., Kneizys, F. X., Chetwynd, J. H., and Shettle, E. P.: AFGL atmospheric constituent profiles, Environ. Res. Pap, 954, 1–46, 1986.

Asner, G. P.: Biophysical and Biochemical Sources of Variability in Canopy Reflectance, Remote Sens. Environ., 64, 234–253, https://doi.org/10.1016/S0034-4257(98)00014-5, 1998.

Atzberger, C.: Object-based retrieval of biophysical canopy variables using artificial neural nets and radiative transfer models, Remote Sens. Environ, 93, 53–67, https://doi.org/10.1016/j.rse.2004.06.016, 2004.

Baldocchi, D. D., Wilson, K. B., and Gu, L.: How the environment, canopy structure and canopy physiological functioning influence carbon, water and energy fluxes of a temperate broad-leaved deciduous forest—an assessment with the biophysical model CANOAK, Tree Physiol., 22, 1065–1077, https://doi.org/10.1093/treephys/22.15-16.1065, 2002.

Berk, A., Conforti, P., Kennett, R., Perkins, T., Hawes, F., and van den Bosch, J.: MODTRAN® 6: A major upgrade of the MODTRAN® radiative transfer code, in: 2014 6th workshop on hyperspectral image and signal processing: Evolution in remote sensing (WHISPERS), pp. 1–4, https://doi.org/10.1109/WHISPERS.2014.8077573, 2014.

Betts, R. A.: Offset of the potential carbon sink from boreal forestation by decreases in surface albedo, Nature, 408, 187–190, https://doi.org/10.1038/35041545, 2000.

Bohren, C. F.: Multiple scattering of light and some of its observable consequences, Am. J. Phys, 55, 524–533, 1987.

Bounoua, L., DeFries, R., Collatz, G. J., Sellers, P., and Khan, H.: Effects of land cover conversion on surface climate, Clim. Change, 52, 29–64, https://doi.org/10.1023/A:1013051420309, 2002.

Bowker, D. E.: Spectral reflectances of natural targets for use in remote sensing studies, vol. 1139, NASA, 1985.

Bréda, N. J. J.: Ground-based measurements of leaf area index: a review of methods, instruments and current controversies, J. Exp. Bot., 54, 2403–2417, https://doi.org/10.1093/jxb/erg263, 2003.

Buras, R., Dowling, T., and Emde, C.: New secondary-scattering correction in DISORT with increased efficiency for forward scattering, J. Quant. Spectrosc. Radiat. Transfer, 112, 2028–2034, https://doi.org/10.1016/j.jqsrt.2011.03.019, 2011.

Cerasoli, S., Yin, J., and Porporato, A.: Cloud cooling effects of afforestation and reforestation at midlatitudes, PNAS, 118, e2026241 118, https://doi.org/10.1073/pnas.2026241118, 2021.

Coddington, O. M., Richard, E. C., Harber, D., Pilewskie, P., Woods, T. N., Chance, K., Liu, X., and Sun, K.: The TSIS-1 Hybrid Solar Reference Spectrum, Geophys. Res. Let., 48, e2020GL091 709, https://doi.org/10.1029/2020GL091709, 2021.

Damm, A., Guanter, L., Verhoef, W., Schläpfer, D., Garbari, S., and Schaepman, M. E.: Impact of varying irradiance on vegetation indices and chlorophyll fluorescence derived from spectroscopy data, Remote Sens. Environ., 156, 202–215, https://doi.org/10.1016/j.rse.2014.09.031, 2015.

Davidson, A. and Wang, S.: The effects of sampling resolution on the surface albedos of dominant land cover types in the North American boreal region, Remote Sens. Environ., 93, 211–224, https://doi.org/10.1016/j.rse.2004.07.005, 2004.

Davidson, A. and Wang, S.: Spatiotemporal variations in land surface albedo across Canada from MODIS observations, C. J. Remote Sens., 31, 377–390, https://doi.org/10.5589/m05-021, 2005.

https://doi.org/10.5194/egusphere-2024-3614
Preprint. Discussion started: 11 December 2024

Deering, D. W. and Eck, T. F.: Atmospheric optical depth effects on angular anisotropy of plant canopy reflectance, Int. J. Remote Sens., 8, 893–916, 1987.

Dye, D. G.: Spectral composition and quanta-to-energy ratio of diffuse photosynthetically active radiation under diverse cloud conditions, J. Geophys. Res. Atmos., 109, https://doi.org/10.1029/2003JD004251, 2004.

Emde, C., Buras-Schnell, R., Kylling, A., Mayer, B., Gasteiger, J., Hamann, U., Kylling, J., Richter, B., Pause, C., Dowling, T., and Bugliaro, L.: The libRadtran software package for radiative transfer calculations (version 2.0.1), Geosci. Model Dev., 9, 1647–1672, https://doi.org/10.5194/gmd-9-1647-2016, 2016.

Eugster, W., Rouse, W. R., Pielke Sr, R. A., Mcfadden, J. P., Baldocchi, D. D., Kittel, T. G. F., Chapin III, F. S., Liston, G. E., Vidale, P. L., Vaganov, E., and Chambers, S.: Land–atmosphere energy exchange in Arctic tundra and boreal forest: available data and feedbacks to climate, Global Change Biol., 6, 84–115, https://doi.org/10.1046/j.1365-2486.2000.06015.x, 2000.

Frisch, S., Shupe, M., Djalalova, I., Feingold, G., and Poellot, M.: The retrieval of stratus cloud droplet effective radius with cloud radars, J. Atmos. Oceanic Technol., 19, 835 – 842, https://doi.org/10.1175/1520-0426(2002)019<0835:TROSCD>2.0.CO;2, 2002.

Gasteiger, J., Emde, C., Mayer, B., Buras, R., Buehler, S., and Lemke, O.: Representative wavelengths absorption parameterization applied to satellite channels and spectral bands, J. Quant. Spectrosc. Radiat. Transfer, 148, 99–115, https://doi.org/10.1016/j.jqsrt.2014.06.024, 2014.

Goel, N. S.: Models of vegetation canopy reflectance and their use in estimation of biophysical parameters from reflectance data, Remote Sens. Rev., 4, 1–212, https://doi.org/10.1080/02757258809532105, 1988.

Goel, N. S. and Strebel, D. E.: Simple beta distribution representation of leaf orientation in vegetation canopies, Agro. J., 76, 800–802, https://doi.org/10.2134/agronj1984.00021962007600050021x, 1984.

Grant, L.: Diffuse and specular characteristics of leaf reflectance, Remote Sens. Environ., 22, 309–322, https://doi.org/10.1016/0034-4257(87)90064-2, 1987.

Grenfell, T. C. and Perovich, D. K.: Incident spectral irradiance in the Arctic Basin during the summer and fall, J. Geophys. Res. Atmos., 113, https://doi.org/10.1029/2007JD009418, 2008.

Henniger, H., Bohn, F. J., Schmidt, K., and Huth, A.: A new approach combining a multilayer radiative transfer model with an individual-based forest model: Application to boreal forests in Finland, Remote Sens., 15, https://doi.org/10.3390/rs15123078, 2023.

Houborg, R. and Boegh, E.: Mapping leaf chlorophyll and leaf area index using inverse and forward canopy reflectance modeling and SPOT reflectance data, Remote Sens. Environ., 112, 186–202, https://doi.org/10.1016/j.rse.2007.04.012, 2008.

Hovi, A., Lukeš, P., and Rautiainen, M.: Seasonality of albedo and FAPAR in a boreal forest, Agric. For. Meteorol., 247, 331–342, https://doi.org/10.1016/j.agrformet.2017.08.021, 2017.

Irvine, W. M. and Pollack, J. B.: Infrared optical properties of water and ice spheres, Icarus, 8, 324–360, https://doi.org/10.1016/0019-1035(68)90083-3, 1968.

Jones, H. G. and Vaughan, R. A.: Remote sensing of vegetation: principles, techniques, and applications, Oxford University Press, USA, 2010.

Kokhanovsky, A. A.: Light scattering reviews 4: single light scattering and radiative transfer, Springer Science & Business Media, 2009.

Kötz, B., Schaepman, M., Morsdorf, F., Bowyer, P., Itten, K., and Allgöwer, B.: Radiative transfer modeling within a heterogeneous canopy for estimation of forest fire fuel properties, Remote Sens. Environ., 92, 332–344, https://doi.org/10.1016/j.rse.2004.05.015, 2004.

Kubelka, P.: Ein Beitrag zur Optik der Farbanstriche, Z. tech. Phys, 12, 593–601, 1931.

https://doi.org/10.5194/egusphere-2024-3614
Preprint. Discussion started: 11 December 2024

Liang, X.-Z., Xu, M., Gao, W., Kunkel, K., Slusser, J., Dai, Y., Min, Q., Houser, P. R., Rodell, M., Schaaf, C. B., and Gao, F.: Development of land surface albedo parameterization based on Moderate Resolution Imaging Spectroradiometer (MODIS) data, J. Geophys. Res. Atmos., 110, D11 107, https://doi.org/10.1029/2004JD005579, 2005.

Liu, C. H., Chen, A. J., and Liu, G. R.: Variability of the bare soil albedo due to different solar zenith angles and atmospheric haziness, Int. J. Remote Sens., 15, 2531–2542, 1994.

Loveland, T. R. and Belward, A. S.: The IGBP-DIS global 1km land cover data set, DISCover: First results, Int. J. Remote Sens., 18, 3289–3295, https://doi.org/10.1080/014311697217099, 1997.

Lucht, W., Schaaf, C., and Strahler, A.: An algorithm for the retrieval of albedo from space using semiempirical BRDF models, IEEE Trans. Geosci. Remote Sens., 38, 977–998, https://doi.org/10.1109/36.841980, 2000.

Lyapustin, A. I. and Privette, J. L.: A new method of retrieving surface bidirectional reflectance from ground measurements: Atmospheric sensitivity study, J. Geophys. Res. Atmos., 104, 6257–6268, https://doi.org/10.1029/1998JD200123, 1999.

Majasalmi, T. and Rautiainen, M.: The impact of tree canopy structure on understory variation in a boreal forest, For. Ecol. Manage., 466, 118 100, https://doi.org/10.1016/j.foreco.2020.118100, 2020.

Martonchik, J. V., Bruegge, C. J., and Strahler, A. H.: A review of reflectance nomenclature used in remote sensing, Remote Sens. Rev., 19, 9–20, https://doi.org/10.1080/02757250009532407, 2009.

Mie, G.: Beiträge zur Optik trüber Medien, speziell kolloidaler Metallösungen, Ann. Phys., 330, 377–445, https://doi.org/10.1002/andp.19083300302, 1908.

Min, Q.: Impacts of aerosols and clouds on forest-atmosphere carbon exchange, J. Geophys. Res. Atmos., 110, https://doi.org/10.1029/2004JD004858, 2005.

Monsi, M.: Uber den Lichtfaktor in den Pflanzengesellschaften und seine Bedeutung fur die Stoffproduktion, Jap. J. Bot., 14, 22–52, 1953.

Myhre, G., Kvalevåg, M. M., and Schaaf, C. B.: Radiative forcing due to anthropogenic vegetation change based on MODIS surface albedo data, Geophys. Res. Let., 32, https://doi.org/10.1029/2005GL024004, 2005.

Nemani, R. R., Keeling, C. D., Hashimoto, H., Jolly, W. M., Piper, S. C., Tucker, C. J., Myneni, R. B., and Running, S. W.: Climate-driven increases in global terrestrial net primary production from 1982 to 1999, Science, 300, 1560–1563, https://doi.org/10.1126/science.1082750, 2003.

Ollinger, S. V.: Sources of variability in canopy reflectance and the convergent properties of plants, New Phytol., 189, 375–394, https://doi.org/10.1111/j.1469-8137.2010.03536.x, 2011.

Pierce, L. L. and Running, S. W.: Rapid estimation of coniferous forest leaf area index using a portable integrating radiometer, Ecology, 69, 1762–1767, https://doi.org/10.2307/1941154, 1988.

Pisek, J., Diaz-Pines, E., Matteucci, G., Noe, S., and Rebmann, C.: On the leaf inclination angle distribution as a plant trait for the most abundant broadleaf tree species in Europe, Agric. For. Meteorol., 323, 109 030, https://doi.org/10.1016/j.agrformet.2022.109030, 2022.

Qin, H., Wang, C., Zhao, K., and Xi, X.: Estimation of the fraction of absorbed photosynthetically active radiation (fPAR) in maize canopies using LiDAR data and hyperspectral imagery, Plos one, 13, e0197 510, 2018.

Ranson, K. J., Biehl, L. L., and Bauer, M. E.: Variation in spectral response of soybeans with respect to illumination, view and canopy geometry, Int. J. Remote Sens., 6, 1827–1842, 1985.

Roderick, M. L., Farquhar, G. D., Berry, S. L., and Noble, I. R.: On the direct effect of clouds and atmospheric particles on the productivity and structure of vegetation, Oecologia, 129, 21–30, 2001.

Schaepman-Strub, G., Schaepman, M. E., Painter, T. H., Dangel, S., and Martonchik, J. V.: Reflectance quantities in optical remote sensing—definitions and case studies, Remote Sen. Environ., 103, 27–42, https://doi.org/10.1016/j.rse.2006.03.002, 2006.

Shettle, E.: Models of aerosols, clouds and precipitation for atmospheric propagation studies, in: Atmospheric propagation in the uv, visible, ir and mm-region and related system aspects, no. 454 in AGARD Conference Proceedings, 1989.

Sinoquet, H., Le Roux, X., Adam, B., Ameglio, T., and Daudet, F. A.: RATP: a model for simulating the spatial distribution of radiation absorption, transpiration and photosynthesis within canopies: application to an isolated tree crown, Plant Cell. Environ., 24, 395–406, https://doi.org/10.1046/j.1365-3040.2001.00694.x, 2001.

Stamnes, K., Tsay, S.-C., Wiscombe, W., and Jayaweera, K.: Numerically stable algorithm for discrete-ordinate-method radiative transfer in multiple scattering and emitting layered media, Appl. Opt., 27, 2502–2509, https://doi.org/10.1364/AO.27.002502, 1988.

Stapf, J., Ehrlich, A., Jäkel, E., Lüpkes, C., and Wendisch, M.: Reassessment of shortwave surface cloud radiative forcing in the Arctic: consideration of surface-albedo–cloud interactions, Atmos. Chem. Phys., 20, 9895–9914, https://doi.org/10.5194/acp-20-9895-2020, 2020.

Stenberg, P., Lukeš, P., Rautiainen, M., and Manninen, T.: A new approach for simulating forest albedo based on spectral invariants, Remote Sens. Environ., 137, 12–16, https://doi.org/10.1016/j.rse.2013.05.030, 2013.

Stephens, G. L.: Remote sensing of the lower atmosphere, an introduction, Oxford University Press, New York, 1994.

Stuckens, J., Somers, B., Delalieux, S., Verstraeten, W. W., and Coppin, P.: The impact of common assumptions on canopy radiative transfer simulations: A case study in Citrus orchards, J. Quant. Spectrosc. Radiat. Transfer, 110, 1–21, https://doi.org/10.1016/j.jqsrt.2008.09.001, 2009.

Verhoef, W.: Light scattering by leaf layers with application to canopy reflectance modeling: The SAIL model, Remote Sens. Environ., 16, 125–141, https://doi.org/10.1016/0034-4257(84)90057-9, 1984.

Verhoef, W.: Theory of radiative transfer models applied in optical remote sensing of vegetation canopies, Ph.D. thesis, Wageningen University and Research, 1998.

Verhoef, W., van der Tol, C., and Middleton, E. M.: Hyperspectral radiative transfer modeling to explore the combined retrieval of biophysical parameters and canopy fluorescence from FLEX – Sentinel-3 tandem mission multi-sensor data, Remote Sens. Environ., 204, 942–963, https://doi.org/10.1016/j.rse.2017.08.006, 2018.

Verrelst, J., Rivera, J. P., van der Tol, C., Magnani, F., Mohammed, G., and Moreno, J.: Global sensitivity analysis of the SCOPE model: What drives simulated canopy-leaving sun-induced fluorescence?, Remote Sens. Environ., 166, 8–21, https://doi.org/10.1016/j.rse.2015.06.002, 2015.

Vicari, M. B., Pisek, J., and Disney, M.: New estimates of leaf angle distribution from terrestrial LiDAR: Comparison with measured and modelled estimates from nine broadleaf tree species, Agric. For. Meteorol., 264, 322–333, https://doi.org/10.1016/j.agrformet.2018.10.021, 2019.

Vilfan, N., van der Tol, C., Muller, O., Rascher, U., and Verhoef, W.: Fluspect-B: A model for leaf fluorescence, reflectance and transmittance spectra, Remote Sens. Environ., 186, 596–615, https://doi.org/10.1016/j.rse.2016.09.017, 2016.

Vilfan, N., Van der Tol, C., Yang, P., Wyber, R., Malenovský, Z., Robinson, S. A., and Verhoef, W.: Extending Fluspect to simulate xanthophyll driven leaf reflectance dynamics, Remote Sens. Environ., 211, 345–356, https://doi.org/10.1016/j.rse.2018.04.012, 2018.

Wan, L., Zhu, J., Du, X., Zhang, J., Han, X., Zhou, W., Li, X., Liu, J., Liang, F., He, Y., and Cen, H.: A model for phenotyping crop fractional vegetation cover using imagery from unmanned aerial vehicles, J. Exp. Bot., 72, 4691–4707, https://doi.org/10.1093/jxb/erab194, 2021.

Warren, S. G.: Optical properties of snow, Rev. Geophys., 20, 67–89, https://doi.org/10.1029/RG020i001p00067, 1982.

https://doi.org/10.5194/egusphere-2024-3614
Preprint. Discussion started: 11 December 2024

Watson, D. J.: Comparative physiological studies on the growth of field crops: I. Variation in net assimilation rate and leaf area between species and varieties, and within and between years, Ann. Bot., 11, 41–76, 1947.

Weihs, P., Lenoble, J., Blumthaler, M., Martin, T., Seckmeyer, G., Philipona, R., De la Casiniere, A., Sergent, C., Gröbner, J., Cabot, T., Masserot, D., Pichler, T., Pougatch, E., Rengarajan, G., Schmucki, D., and Simic, S.: Modeling the effect of an inhomogeneous surface albedo on incident UV radiation in mountainous terrain: Determination of an effective surface albedo, Geophys. Res. Lett., 28, 3111–3114, https://doi.org/10.1029/2001GL012986, 2001.

Wendisch, M. and Yang, P.: Theory of atmospheric radiative transfer: A comprehensive introduction, Wiley, ISBN 9783527408368, 2012.

Wendisch, M., Pilewskie, P., Jäkel, E., Schmidt, S., Pommier, J., Howard, S., Jonsson, H. H., Guan, H., Schröder, M., and Mayer, B.: Airborne measurements of areal spectral surface albedo over different sea and land surfaces, J. Geophys. Res. Atmos., 109, https://doi.org/10.1029/2003JD004392, 2004.

Wiscombe, W. J. and Warren, S. G.: A model for the spectral albedo of snow. I: pure snow, J. Atmos. Sci., 37, 2712 – 2733, https://doi.org/10.1175/1520-0469(1980)037<2712:AMFTSA>2.0.CO;2, 1980.

Yan, H., Wang, S., Dai, J., Wang, J., Chen, J., and Shugart, H. H.: Forest greening increases land surface albedo during the main growing period between 2002 and 2019 in China, J. Geophys. Res. Atmos., 126, e2020JD033 582, https://doi.org/10.1029/2020JD033582, 2021.

Yang, P., Verhoef, W., and van der Tol, C.: The mSCOPE model: A simple adaptation to the SCOPE model to describe reflectance, fluorescence and photosynthesis of vertically heterogeneous canopies, Remote Sens. Environ., 201, 1–11, https://doi.org/10.1016/j.rse.2017.08.029, 2017.

Yang, P., van der Tol, C., Yin, T., and Verhoef, W.: The SPART model: A soil-plant-atmosphere radiative transfer model for satellite measurements in the solar spectrum, Remote Sens. Environ., 247, 111 870, https://doi.org/10.1016/j.rse.2020.111870, 2020.

Yang, P., Prikaziuk, E., Verhoef, W., and van der Tol, C.: SCOPE 2.0: a model to simulate vegetated land surface fluxes and satellite signals, Geosci. Model Dev., 14, 4697–4712, https://doi.org/10.5194/gmd-14-4697-2021, 2021.

Yang, X., Li, R., Jablonski, A., Stovall, A., Kim, J., Yi, K., Ma, Y., Beverly, D., Phillips, R., Novick, K., Xu, X., and Lerdau, M.: Leaf angle as a leaf and canopy trait: Rejuvenating its role in ecology with new technology, Ecol. Lett., 26, 1005–1020, https://doi.org/10.1111/ele.14215, 2023.

Zheng, L., Zhao, G., Dong, J., Ge, Q., Tao, J., Zhang, X., Qi, Y., Doughty, R. B., and Xiao, X.: Spatial, temporal, and spectral variations in albedo due to vegetation changes in China's grasslands, ISPRS J. Photogramm. Remote Sens., 152, 1–12, https://doi.org/10.1016/j.isprsjprs.2019.03.020, 2019.